J. Fluid Mech. (1973), *vol.* 59, *part* 2, *pp.* 281–335
Printed in Great Britain

On transition in a pipe. Part 1. The origin of puffs and slugs and the flow in a turbulent slug

By I. J. WYGNANSKI† AND F. H. CHAMPAGNE‡
Boeing Scientific Research Laboratory, Seattle, Washington

(Received 20 July 1972)

Conditionally sampled hot-wire measurements were taken in a pipe at Reynolds numbers corresponding to the onset of turbulence. The pipe was smooth and carefully aligned so that turbulent slugs appeared naturally at $Re > 5 \times 10^4$. Transition could be initiated at lower Re by introducing disturbances into the inlet. For smooth or only slightly disturbed inlets, transition occurs as a result of instabilities in the boundary layer long before the flow becomes fully developed in the pipe. This type of transition gives rise to turbulent slugs which occupy the entire cross-section of the pipe, and they grow in length as they proceed downstream. The leading and trailing 'fronts' of a turbulent slug are clearly defined. A unique relation seems to exist between the velocity of the interface and the velocity of the fluid by which relaminarization of turbulent fluid is prevented. The length of slugs is of the same order of magnitude as the length of the pipe, although the lengths of individual slugs differ at the same flow conditions. The structure of the flow in the interior of a slug is identical to that in a fully developed turbulent pipe flow. Near the interfaces, where the mean motion changes from a laminar to a turbulent state, the velocity profiles develop inflexions. The total turbulent intensity near the interfaces is very high and it may reach 15 % of the velocity at the centre of the pipe. A turbulent energy balance was made for the flow near the interfaces. All of the terms contributing to the energy balance must vanish identically somewhere on the interface if that portion of the interface does not entrain non-turbulent fluid. It appears that diffusion which also includes pressure transport is the most likely mechanism by which turbulent energy can be transferred to non-turbulent fluid. The dissipation term at the interface is negligible and increases with increasing turbulent energy towards the interior of the slug.

Mixed laminar and turbulent flows were observed far downstream for

$$2000 < Re < 2700$$

when a large disturbance was introduced into the inlet. The flow in the vicinity of the inlet, however, was turbulent at much lower Re. The turbulent regions which are convected downstream at a velocity which is slightly smaller than the average velocity in the pipe we shall henceforth call puffs. The leading front of a puff does not have a clearly defined interface and the trailing front is clearly

† Present address: School of Engineering, Tel-Aviv University.
‡ Present address: Department of Applied Mechanics and Engineering Sciences, University of California, San Diego.

defined only in the vicinity of the centre-line. The length and structure of the puff is independent of the character of the obstruction which created it, provided that the latter is big enough to produce turbulent flow at the inlet. The puff will be discussed in more detail later.

---

1. Introduction

An area of special interest in fluid mechanics is transition from laminar to turbulent flow. A fundamental understanding of the mechanics of transition in general is far from complete, although significant advances have been made in the past ten years. One of the outstanding questions remaining pertains to the final stage of the transition process – the growth of turbulent spots. The mechanism by which steep gradients of vorticity are maintained at the interfaces of turbulent spots or regions and the concomitant process of entrainment of fluid into a turbulent region are poorly understood, even though they exist in all turbulent shear flows with a free interface. As a first attempt to obtain detailed information on turbulent–non-turbulent interfaces and entrainment, it seemed advisable to choose a flow in which the interfaces are well defined, and therefore relatively simple to detect. After examining various available flows, it appeared that the study of turbulent slugs occurring in the transition process in pipe flow was most suitable. Previous observations of transitional flow in a pipe had shown that the frequency and length of the slugs could be changed by making small variations in the velocity of the fluid in a given pipe. The control over the frequency and length of the slugs provided strong motivation for choosing this flow for our first study of turbulent–non-turbulent interfaces and the growth and dynamics of turbulent regions.

The first systematic investigation of a pipe flow was conducted by Reynolds (1883), who discovered the law of similarity which now bears his name. Reynolds stated that, for a given pipe and fluid, a critical velocity U_c at which the resistance (or pressure drop) changes its value exists. This result helped to determine a dimensionless parameter $U_c D/\nu \approx 2000$ (where D is the diameter of the pipe and ν is the kinematic viscosity of the fluid), which is commonly referred to as the critical Reynolds number. Below the critical Reynolds number no sinuous motion is expected to sustain itself regardless of the initial disturbance. Reynolds also observed that "... there were two critical values for the velocity in the tube, the one at which steady motion changed into eddies, the other at which eddies changed into steady motion". The number $Re_c \approx 2000$ corresponds to the latter critical velocity, because it was obtained for a tube which had a valve placed at its entrance. The critical Reynolds number of approximately 2000 does *not* represent the lower bound at which natural transition from laminar to turbulent flow occurs, but rather a critical Reynolds number at which turbulent flow, once established, can intermittently be maintained in a long pipe. This point will be elaborated further.

Reynolds also first observed the intermittent character of transition and his own description of the phenomenon may be quoted.

"Another phenomenon very marked in smaller tubes was the intermittent

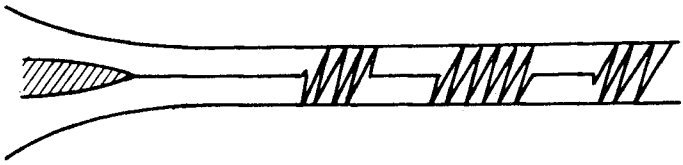

FIGURE 1. The intermittent character of transition as shown by Reynolds.

character of the disturbance. The disturbance would suddenly come on through a certain length of the tube and pass away and then come on again, giving the appearance of flashes, and these flashes would often commence successively at one point in the pipe. The appearance when the flashes succeeded each other rapidly was as shown" [...in figure 1].

The study of pipe flow has occupied many researchers from the time of Reynolds until now, so it is impossible to cite every paper on the subject. We shall attempt to mention some of the papers which are most relevant to the present investigation.

When fluid enters a pipe from a large settling chamber through a smooth contraction, the radial distribution of velocity in the entrance region changes with downstream distance. Initially the velocity profile is nearly uniform, but because of viscous effects, the profiles vary with downstream distance, until a cross-section is reached where a fully developed velocity profile is attained. From this cross-section onwards the flow is independent of the downstream co-ordinate.

The initial inlet length may extend several hundred diameters if the flow in the pipe is laminar. Goldstein (1938, p. 304) and more recently Christiansen & Lemmon (1965) calculated the laminar velocity profile at the inlet by using steady-state boundary-layer equations. Tatsumi (1952) calculated the entrance profile and then applied linear stability theory to his calculation. He found the flow in the inlet region of the pipe to be unstable to small axisymmetric disturbances in contrast to the fact that fully developed Poiseuille flow is stable to such disturbances. The analyses of Tatsumi and of Smith (1960) determine the critical Reynolds number and the location along the pipe where instability is most likely to occur. Because of the presence of a core of constant velocity one would expect turbulent spots to originate near the wall, where the mean shear is high, just as in a boundary layer. According to Kovasznay, Komoda & Vesudeva (1962) regions of highly concentrated vorticity occur near the outer edge of a boundary layer at the initial stages of transition. A characteristic feature of these regions is a 'spike' on a trace of a linearized hot-wire output. A spike of sufficiently large amplitude may burst into a turbulent spot (Elder 1960). As the spot travels downstream it may increase in size until its dimension becomes comparable with the radius of the pipe (Lindgren 1969). The result is a turbulent slug, temporarily filling the entire cross-section of the pipe with turbulent flow. The slug is restricted by the pipe diameter and can only grow in the axial direction. Far from the inlet the pipe geometry exerts a major influence on the structure of the slug, and one would expect the interior of the slug to behave in much the same manner as the fully developed turbulent pipe flow (Wygnanski 1971).

The evolution of turbulent regions in birefringent liquid (bentonite sol) was

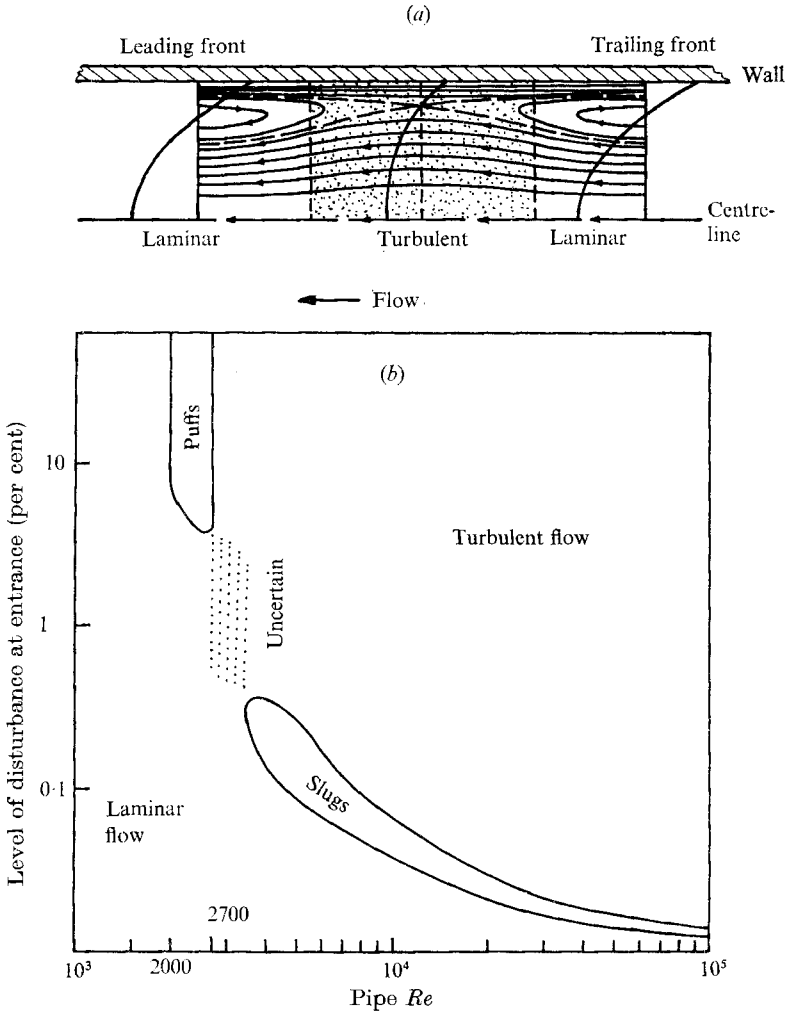

FIGURE 2. (*a*) Schematic diagram of the flow in a turbulent slug after Coles (1962). (*b*) The regions in which slugs and puffs occur in transitional pipe flow as a function of the disturbance level.

investigated by Lindgren and presented in a series of articles in *Arkiv für Fysik* from 1954 to 1963. The observations were made using optical methods or pressure records on the surface of the pipe, so the data provide very little information on the flow in the interior of the region or near the turbulent–non-turbulent interfaces. The results concerned with the propagation velocity of individual turbulent regions at various inlet conditions (and thus different *Re*) are, nevertheless, useful. Lindgren showed that only the turbulent regions of natural origin increase in length as they proceed down the pipe. Turbulent regions created by large disturbances at the inlet tend, sometimes, to split and decay.

Rotta (1956) determined the intermittency factor and the frequency of the turbulent regions on the basis of the difference between the mean momentum in laminar and turbulent flow. He also estimated the overall fluid velocity in the

turbulent and laminar zones by scaling strip chart recordings of hot-wire output. Patel & Head (1969) measured mean velocity profiles in an intermittently turbulent flow in a circular pipe and a two-dimensional channel. Since no distinction was made between the turbulent and laminar regimes, only the deviations from the 'law of wall' could be assessed and criteria for fully developed turbulent pipe flow could be set up.

As a result of some of these observations, Coles (1962) proposed to view the intermittency in a pipe flow as alternation between fully developed laminar and turbulent regimes. This view enabled Coles to represent schematically the mean flow in the vicinity of the interface as shown in figure 2 (*a*). The streamline pattern was based on an assumption that both leading and trailing fronts propagate downstream with a velocity equal to the average speed of the fluid (volume flow/area). However, this is inconsistent with the general observations made in boundary-layer spots (Shubauer & Klebanoff 1956), and fails to explain the growth or splitting of the turbulent regions. In most turbulent free shear flows, moreover, a body of fluid remains turbulent after being entrained into the turbulent regime. The rapid transition of the fluid from laminar to turbulent and then back to laminar flow as shown in figure 2 (*a*) requires unscrambling of vorticity which was not hitherto encountered.

We found two very different types of intermittently turbulent flow occurring naturally in a pipe. (i) Slugs, which are caused by the instability of the boundary layer to small disturbances in the inlet region of the pipe. (ii) Puffs, which are generated by large disturbances at the inlet.

While slugs are associated with transition from laminar to turbulent flow, puffs represent an incomplete relaminarization process. Puffs can only be seen at $2000 \leqslant Re \leqslant 2700$, while slugs occur at any $Re \geqslant 3200$. In figure 2 (*b*) the Reynolds numbers at which puffs and slugs occur are delineated as a function of the disturbance level at the entrance. The figure represents schematically the various regions encountered in transitional pipe flow at large distances from the inlet. Because the ordinate does not uniquely determine the Re at which transition occurs, the numbers shown may be regarded as a guide only. The region where slugs occur in the figure moves to the right with decreasing distance from the inlet. In the following pages we present some observations on transition in a pipe with particular emphasis on the flow in a turbulent slug.

2. Description of the apparatus and experimental techniques

A seamless aluminum pipe of diameter of 3·3 cm and a total length of approximately 500 diameters was used in the experiment. It consisted of five sections which were faced squarely on a precision lathe, threaded and joined to one another by brass couplings. The five sections were chosen out of approximately 100 similar sections in order to minimize and match their eccentricity. Care was taken to avoid any gaps at the joints, and surface discontinuities were virtually eliminated by having the entire pipe honed after it was properly fixed and aligned. The pipe sat in a V-shaped trough made of thick aluminum angle. Screws were threaded through the angle from the outside and pushed against

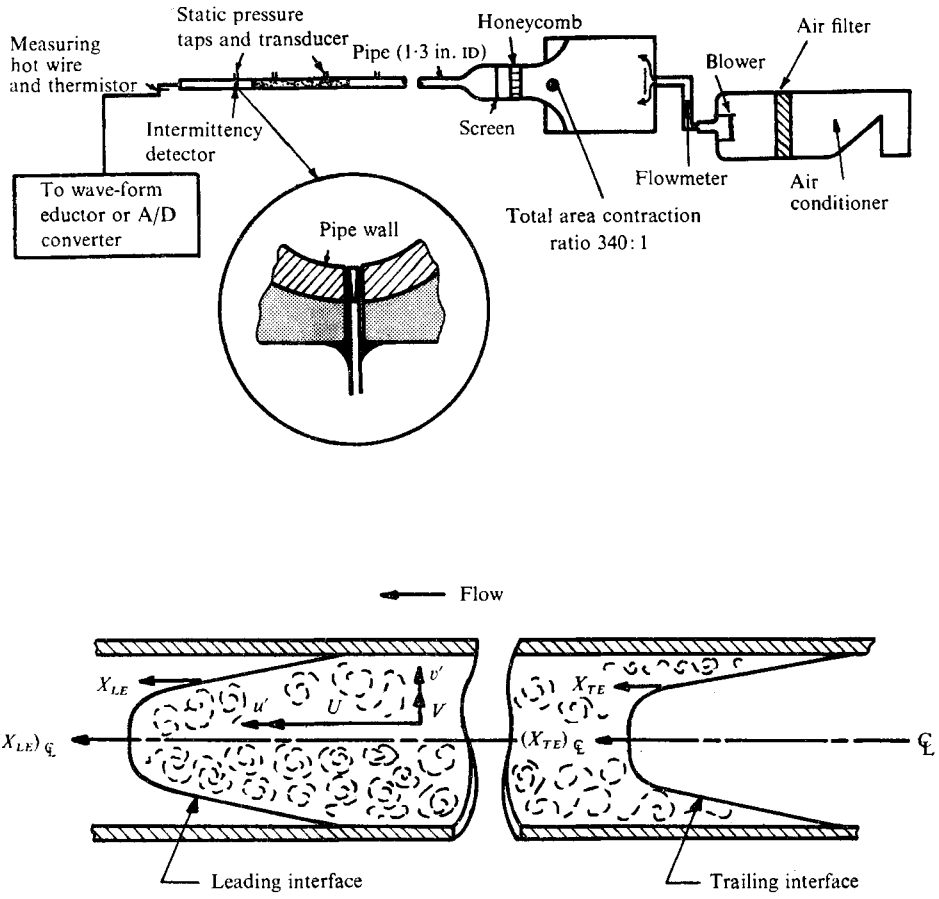

FIGURE 3. A schematic diagram of the apparatus and notation.

the pipe, thus permitting a fine alignment of the pipe. The tolerance on the alignment was better than ± 1 mm over the entire length of the pipe.

A variable-speed blower supplied the flow of air through a flowmeter and a settling chamber to the pipe (figure 3). A large resistance to the flow was maintained between the blower and the settling chamber, thus loading the blower and making it insensitive to the unsteady pressure drop in the pipe. The air was cleaned and precooled by passing through an air conditioner and a filter. The temperature of the flow in the pipe was maintained to within $\pm 1\,^{\circ}$F of the ambient room temperature and the latter did not vary by more than $2\,^{\circ}$F during a whole day. For measurements in purely laminar flow the entire pipe assembly was insulated thermally and no data were taken when the temperature strayed from a prescribed value by more than $0{\cdot}4\,^{\circ}$F. The necessity of maintaining a constant temperature along the entire pipe cannot be overemphasized. Room air-conditioner vents discharging 8 ft away from the bare pipe or a 100 W bulb placed 2 ft away from the uninsulated plenum chamber could distort the parabolic profile beyond recognition.

The settling chamber consisted of two subsections (figure 3) put in tandem

and connected by a smooth contraction. The overall contraction ratio was 340 to 1. Easy access was provided to the smaller settling chamber, into which screens or a deep cell honeycomb could be placed. This access was also used to introduce various obstructions at the pipe inlet. Replacing or removing any of the above-mentioned items from the inlet altered the transition Reynolds number Re_T, i.e. the lowest Re at which turbulent regions were first observed 500 diameters downstream. Thus, one could observe the effect of Re and initial disturbances on the flow. The following cases were studied in some detail.

(i) A honeycomb and a 40-mesh screen in the settling chamber gave

$$Re_T = 45\,000.$$

(ii) The honeycomb alone in the settling chamber gave $Re_T = 17\,500$.

(iii) A cylinder with its axis normal to the flow was placed at the inlet in addition to the honeycomb in the settling chamber. When the diameter of the cylinder was 0·25 in., $Re_T \approx 4000$. In this configuration Re_T could be changed at will between the limits $2000 \leqslant Re_T \leqslant 17\,500$ depending on the diameter of the cylinder.

(iv) An orifice plate having an opening of 0·5 in. when placed at the inlet gave $Re_T = 2000$. Two other orifices with diameters of 1·0 in. and 0·2 in. gave the same Re_T.

(v) A circular thin disk 0·8 in. in diameter was suspended with thin wires in the centre of the pipe, giving $Re_T = 2000$.

Observation ports were provided at various distances from the inlet. The ports were constructed in pairs diametrically opposite one another to enable insertion of two instruments at the same cross-section. When not in use the ports were plugged with carefully contoured and honed brass stoppers. The ports were lined with plastic sleeves which fit snugly to the hot-wire probes, thus preventing any air leaks during measurements. Five static pressure taps (diameter 0·013 in.) were located in the last 12 ft section of the pipe.

Measurements were made with linearized constant-temperature hot-wire anemometers. The wires were calibrated in a wind tunnel at the temperature later used in the pipe. Calibration of the X arrays was rechecked in fully turbulent pipe flow by measuring the shear stress in a number of radial locations and comparing it with the shear stress distribution obtained from the pressure drop. Part of the data was processed by using various analog devices like GPS Model 4040 multipliers, Philbrick/Nexus Model 1003 FET operational amplifiers as differentiators, Princton Applied Research Model TDH-9 Waveform Eductor, etc. All components were calibrated by using known signals for various frequencies up to 20 kHz.

Detection of turbulence was done in the usual manner described in previous papers (e.g. Wygnanski 1971). Almost invariably a hot-wire signal is differentiated, rectified, smoothed, amplified and clipped to produce a step-like signal which would trigger an electronic circuit at two specified levels. Parts of the process are usually repeated one or more times to improve the quality of turbulence detection; this case was no exception.

Some data were processed digitally using a direct on-line computer system.

Signals were sent through Dynamics 7514 amplifiers and shielded coaxial cables to an IBM 1827 and a Model 360-44 computer. The converter read each data point with 14-bit resolution plus a sign bit and could sample at the rate of 18000 times per second. A wave-form eductor program was written for the computer to simulate the analog device. Since the eductor program, or instrument, is not yet in common use, we shall attempt a short description of its operation. After receiving a trigger pulse from the turbulence detector, the A/D converter waits for a prescribed period of time (predetermined in the program) before starting to sample data for another predetermined time period. The total sampling time is subdivided into 1000 equal time periods (the analog instrument has 100 discrete elements only) and the relevant data obtained during each small time interval are processed and stored in a separate memory cell. Running averages of the velocity signal were formed over predetermined time intervals from the data stored in each memory cell. The process is repeated every time a trigger pulse is fed to the clock, so one obtains ensemble-averaged data conditioned in time to the triggering pulse.

A hot wire embedded flush with the surface of the pipe 1 m upstream of the measuring station was used as a turbulence detector, thereby providing a trigger signal in advance of the oncoming turbulent–non-turbulent interface (either leading or trailing front). The data collected at the measuring station thus provided a picture of the flow as it passed through the interface. The sampling procedure depends on the assumption that successive interfaces move downstream at the same velocity, at a given Re, and do not distort as they move from the detector to the measuring station. These assumptions are shown later to be approximately correct, but a small standard deviation from the mean velocity of the turbulent interface tended to smear somewhat the ensemble average of the results and limited the resolution of the data to about two pipe diameters on each side of the interface. (The length of the slugs or the spacing between them could be larger than the entire length of the pipe.) To improve resolution near the interface, a special time-delay network was designed permitting the use of a single signal for the detection and analysis of turbulence. The signal was sent to two separate channels. One (non-delayed) went to the turbulence detector, while the other (delayed) provided the data to be conditioned on the detection of an interface. By delaying the second channel one could recapitulate the signal (representing the flow velocity or its fluctuations about some mean) which existed just before the interface arrived at the measuring station. The results obtained in this manner were free from averaging over the speed and the shape of the interface. The time delay was different for the leading and trailing fronts. For $Re \approx 20000$, delays of 10 and 140 ms were required for the leading and trailing interfaces respectively. An ordinary LC network was useless because of the long time delay involved, and we had to resort to a digital instrument. The signal was transformed into 12 binary bits and each bit was passed through an array of shift registers operated by a clock. Every time a bit was transferred from one register to the next a certain time elapsed. After the required delay had been attained, the 12 bits of information were retransformed into an analog signal. By controlling the clock sampling frequency a signal could be delayed for

a relatively long period of time without distortion and loss of the high-frequency oscillations.

Transitional flow in a pipe is non-stationary because the velocity measured at a given point varies randomly with time depending on whether the local flow is laminar or turbulent. It is convenient to obtain the conventional square of a fluctuating component of a quantity by a capacitive coupling of the signal. If the time constant of the coupling is very large in comparison with the duration of the turbulent regions or the intervals between them the capacitor will charge to an average value representative of the long-time mean velocity. A mean velocity in the turbulent zone, for example, may be different from the long-time mean velocity in the pipe depending on the radial location of the hot-wire probe. The local ensemble-averaged velocity near the interface may again be different from both the conventional mean or the turbulent-zone averaged velocity depending on the distance from the interface considered. Whenever it is desirable to obtain the local average of the square of the fluctuating component, the difference between the conventional mean velocity and the ensemble-averaged local velocity must therefore be taken into account. Corrections of this type are described in some detail by Kibens (1968) and by Wygnanski & Fiedler (1970). If one were certain that no significant energy is contained in the low-frequency oscillations, however, one could shorten the time constant of the capacitive coupling in order that the output would follow the changes in mean velocity between the laminar and turbulent regimes. The above-mentioned corrections could thus be avoided, but the simplification is only possible when the time required for the mean velocity level to change from one value to another (as the interface passes through) is much longer than the characteristic times of the lowest frequency turbulent fluctuations in the flow. The possibility of this simplification was tested by using various high-pass filter settings. For most measurements a filter setting having a flat frequency response between 10 Hz and 10 kHz was found to be adequate. Limiting the low-frequency response and eliminating the corrections resulting from changes in d.c. level gave consistently better repeatable results. Measurement of the radial and azimuthal fluctuations $\overline{v^2}$ and $\overline{w^2}$ gives rise to no difficulty, because the radial velocity associated with the passing of the interface is too small to be measured by an X array. Nevertheless, changing the setting of the high-pass filter from d.c. to 20 Hz did not show different results.

When the data were processed in a digital form, the capacitive coupling was eliminated. The velocity was calculated for each ensemble and the standard deviation was obtained about the running average, so that slight variations in the velocity among the ensembles were not interpreted as turbulent fluctuations. The results were averaged typically over 150–200 ensembles. The results obtained by means of the analog system compared well with those obtained with the aid of the computer.

For purposes of flow visualization a smaller glass tube in which water was used was constructed. A filament of dye was introduced at the centre of the contraction and observed at various distances downstream. At times it was preferable to use pearlessence for flow visualization.

Most of the quantitative results presented were taken at $Re \approx 20000$, but some measurements were also made at $Re = 2300$, 4200 and 50000.

3. Results and discussion

3.1. *The gross characteristics of slugs and puffs*

During a preliminary investigation conducted by the first author at the Technion (Wygnanski 1971) the relation between the conditions at the inlet of the pipe and the character of the turbulent regions emerging far downstream at the pipe outlet was established. Some experiments were repeated in the present experimental set-up in order to re-establish the generality of the previous observations and add quantitative information.

Figure 4 (plate 1) shows some oscillograms of hot-wire output observed at the centre of the pipe $r = 0$ and at $x/D = 505$ (x being the distance measured from the inlet of the pipe and D its interior diameter). The vertical trace is directly proportional to the axial velocity U and time increases from left to right. Figure 4 (*a*) was obtained when a circular cylinder of diameter 0·25 in. was placed at the end of the contraction. The transition Reynolds number was reduced to about 4200 as a result of the disturbance, yet the magnitude of the disturbance was insufficient to trigger turbulence near the entrance of the pipe. One observes a drop in velocity on the centre-line of the pipe as the leading turbulent front passes by. The adjustment is necessary because the turbulent velocity profile is fuller than the laminar profile, yet the average mass flow in the pipe is constant. The transition between laminar and turbulent flows at the beginning and end of the turbulent region is abrupt relative to its duration. The duration of the turbulent region and hence its physical length varies from case to case even though a constant Re is maintained. The average length of the regions is comparable with the length of the pipe. Similar hot-wire traces were observed for $3200 \leqslant Re \leqslant 50000$. The limitation on the high value of Re was imposed by the capacity of the blower, but the lower limit, which is by no means precise, required a larger cylinder at the inlet. With the larger obstruction, the flow could suddenly turn fully turbulent. When the critical Reynolds number was reduced to about 2700 different traces of velocity were observed. They are shown in figures 4 (*b*) and (*c*), and could generally be seen between $2000 \leqslant Re \leqslant 2700$. One may notice that at the centre of the pipe the velocity slowly dropped as the turbulence level increased until a threshold level was attained. Thereafter, the velocity increased quite rapidly while the fluctuation level dropped. When the Re was fairly low, the duration of the occurrence was constant, which is at variance with the previous case. A cumulative trace of 15 such occurrences shown at the bottom of the figure verifies this point. The oscilloscope in this case was triggered externally by a turbulence detector located upstream as described in the previous section.

Looking at the hot-wire output at various radial locations in the pipe (figure 5, plate 2) one can see that the turbulence signature depends greatly on the level of disturbance at the inlet. For highly disturbed inlet flow ($Re = 2360$) the amplitude of the oscillations near the trailing edge of the turbulent region decreases

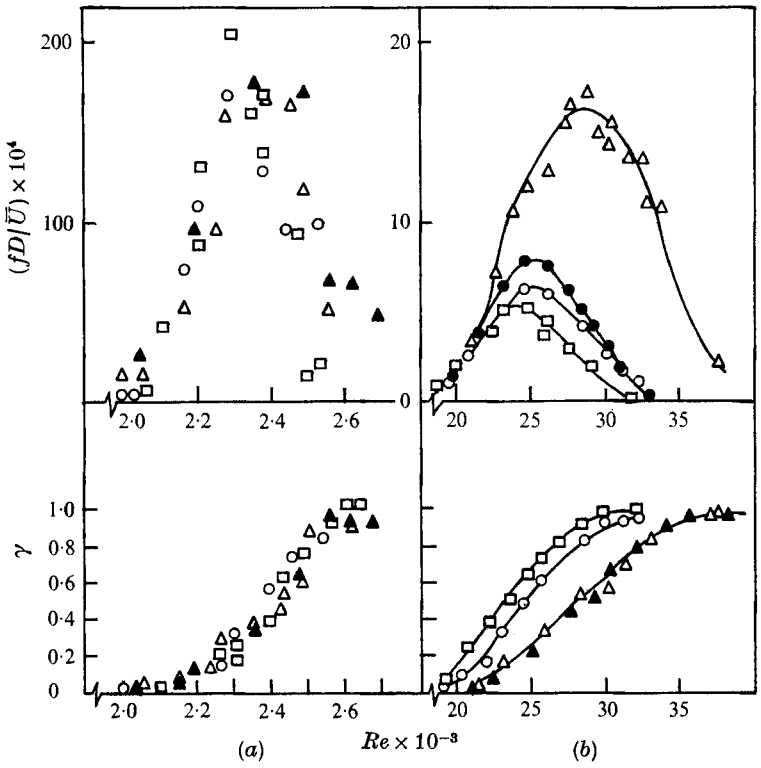

FIGURE 6. Intermittency and frequency of occurrence of (*a*) puffs (highly disturbed entry) and (*b*) slugs (natural transition).

x/D	▲	△	●	○	□
	110	220	330	395	505

as one moves the sensor from the centre-line towards the wall. At $r/R = 0{\cdot}9$ one can only observe a strong spike in the velocity rather than a turbulence signature. On the other hand, when the disturbance at the inlet was reduced ($Re = 4200$) the amplitude of the hot-wire signature near the trailing front increased as the sensor was moved towards the wall (the same holds near the leading front as well). This behaviour is typical of fully turbulent pipe flow. Oscillograms similar to those shown in figure 5 (*b*) were observed at much higher Re (up to $Re = 50000$). Thus, the difference between the signatures in parts (*a*) and (*b*) of this figure can not be attributed purely to Reynolds number effects. It was concluded that the traces shown in figures 4 and 5 represent two distinctly different phenomena occurring during transition in a pipe. We shall refer to the turbulent regions occurring at higher Re as slugs and to the others as puffs. The traces shown by Rotta (1956) and by Patel & Head (1969) represent puffs as they are similar to the puff oscillograms of figures 4 and 5. They occur at the same range of Re and are caused by orifice plates at the inlet of their respective pipes.

The lower part of figure 6 shows the intermittency factor γ as a function of Re at different distances from the inlet of the pipe (γ represents the fraction of the time during which the flow is turbulent). In the upper part of the figure the

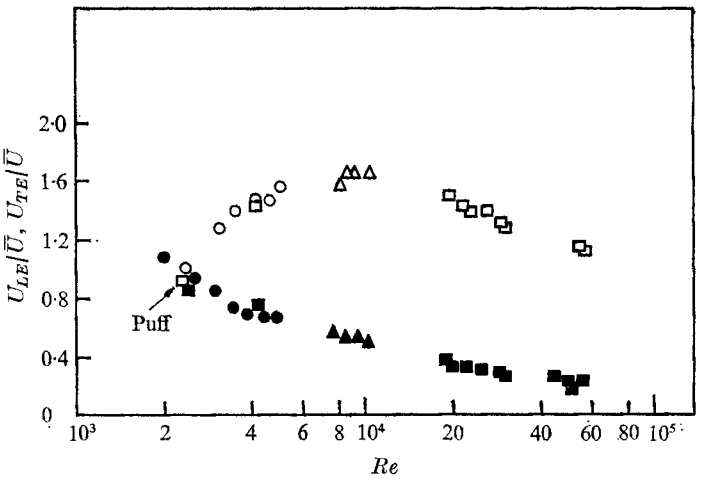

FIGURE 7. The propagation speed of puffs and slugs at various Reynolds numbers. ○, Lindgren (1957); △, Wygnanski (1971); □, present results; – – –, Lindgren (1969) theoretical result for the propagation of the rear boundary at $Re \to \infty$.

frequency f of occurrence of puffs and slugs is plotted against the same variables. Figure 6(*a*) refers to highly disturbed entry, i.e. puffs. No puffs were observed at $Re < 2000$ and the flow was fully turbulent at $Re \geqslant 2700$. These results are in agreement with Valerani (1964) and agree with Rotta (1956). The intermittency factor for a highly disturbed entry is a subjective quantity because the turbulent intensity at the leading front of a puff increases gradually along the puff. Consequently, no importance should be attached to minor differences between the currently reported values of γ and those reported by Rotta. The frequency of the puffs could be evaluated more objectively, especially at the lower Re. The results are in good agreement with the raw data of Rotta which are shown in figure 2 of his paper. We did not observe any reduction in frequency of the puffs with increasing x/D (for $x/D > 100$), nor did we observe any noticeable increase in γ. We disagree with Rotta's conclusion that the frequency of puffs reduces with x/D, although his raw data for $150 \leqslant x/D \leqslant 483$ does not seem to warrant his conclusion. It seems that for $x/D > 100$ the average puff reaches some kind of moving equilibrium with its surrounding flow. The slugs, on the other hand, grow with axial distance and merge with one another as they move downstream. This may be inferred from the fact that γ increases and f decreases with increasing x. In this case the measurement of γ is objective, because a clear-cut turbulent–non-turbulent interface exists at both ends of a slug (figure 4). The results shown in figure 6 are for $Re_T \approx 18\,000$, yet very similar sets of results were reproduced at Reynolds numbers larger than 3200. By measuring the speed of the leading and trailing fronts U_{LE} and U_{TE} respectively, we could assess the actual rate of growth of turbulent slugs with x. The results presented in figure 7 are rendered dimensionless through division by $\overline{U}$, an average velocity over the cross-section of the pipe. The results were obtained by placing two turbulence detectors 1 m apart and flush with the pipe's inner surface and measuring the time required for a turbulent front to travel between them. The measurements were independent of x/D, but

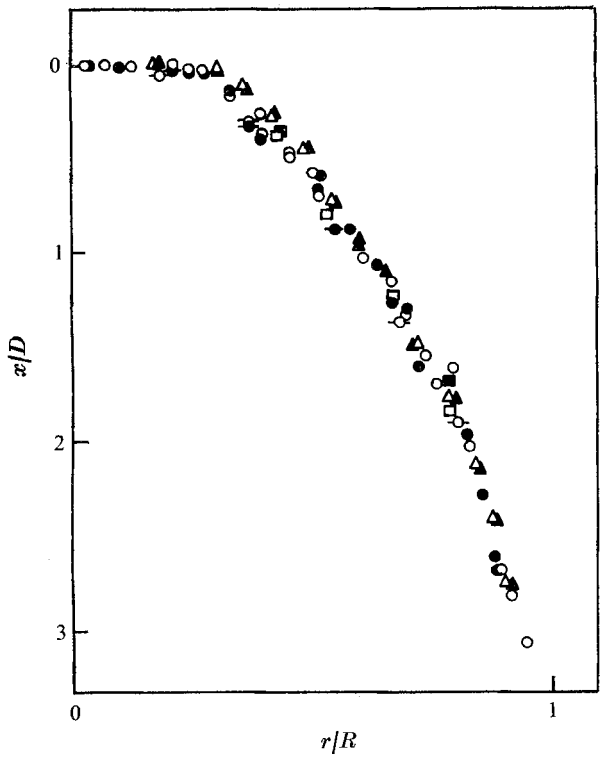

FIGURE 8. The average shape of the interface of a slug. Open and filled symbols represent trailing and leading fronts respectively. Flags indicate data obtained on the other side of the centre-line. ○, $Re = 2{\cdot}32 \times 10^4$, $x/D = 505$; △, $Re = 0{\cdot}42 \times 10^4$, $x/D = 505$; □, $2{\cdot}00 \times 10^4$, $x/D = 395$.

showed dependence on Re_T. The data shown in figure 7 were obtained in three different pipes. The present results overlap those of Lindgren (1957) and extend to much higher Reynolds numbers. The trailing-front velocity continuously decreases with increasing Re, and presumably one would extend the observations to the limit $Re \to \infty$ by stating that the flow has to be fully turbulent because $U_{TE} \to 0$. Lindgren (1969) calculated theoretically the minimum value U_{TE} could reach as $Re \to \infty$. The present experiments do not agree with Lindgren's prediction. The difference between U_{TE} and U_{LE} represents the rate of growth of a slug with x at a given Re. Because the length of a slug is of the same order of magnitude as the length of the pipe and often longer $U_{LE} - U_{TE} \approx \overline{U}$, implying that the slug, during its duration, entrains the total mass flow supplied by the blower. Thus, as $U_{TE} \to 0$, $U_{LE} \to \overline{U}$. Only for puffs $U_{LE} \approx U_{TE}$, implying that they do not grow with distance along the pipe. The dimensionless ratio $U_{LE}/\overline{U}$ has a maximum at $Re \approx 10^4$ and then drops at higher Re.

By keeping one turbulence detector at the centre of the pipe at a given cross-section and moving the other detector, both radially and axially, one may obtain the average shape of a turbulent interface by requiring that the turbulence signatures from both detectors appear simultaneously on the scope. This is a trial-and-error procedure and is not very accurate, because the shape of the interface

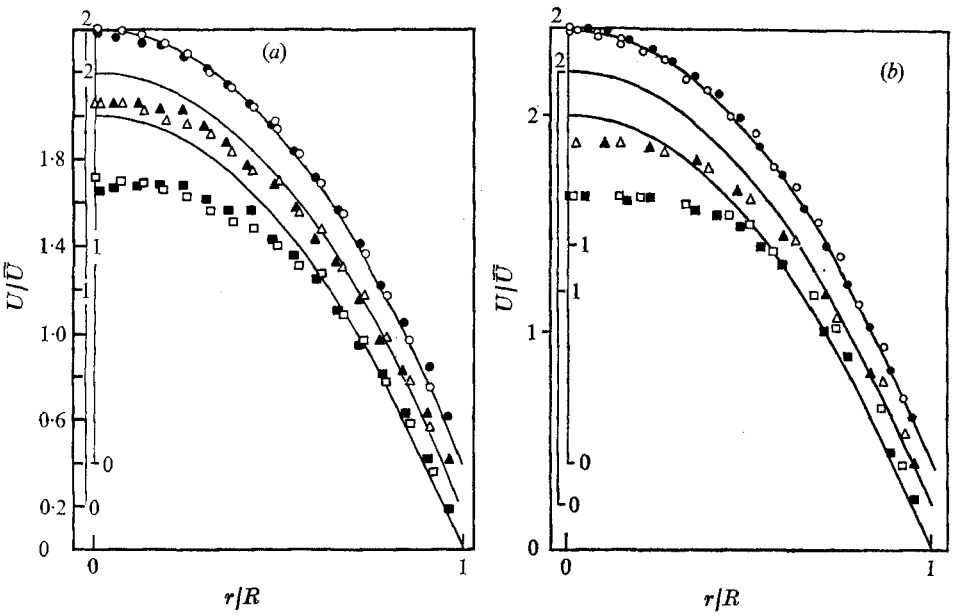

FIGURE 9. Laminar velocity profiles measured at $x/D = 505$ and various Re. ——, $2[1-(r/R)^2]$; shaded symbols represent measurements made on other side of centre-line.

	(*a*) $Re_T = 17{\cdot}5 \times 10^3$			(*b*) $Re_T = 45 \times 10^3$		
	○	△	□	○	△	□
x/D Re	0·133	0·049	0·0308	0·0439	0·0176	0·0123
$Re \times 10^{-3}$	3·8	10·3	16·4	11·5	28·7	41
Re/Re_T	0·217	0·588	0·937	0·255	0·638	0·911

may vary somewhat from slug to slug. The average shape of the interface as obtained by this procedure is shown in figure 8. The interface is blunt at the centre of the pipe, and curves upstream near the wall. In comparison with the average length of the slug, which extends over several hundred pipe diameters, an upstream curvature of some three diameters should have very little effect on the flow in the slug's interior. From figure 8 it may be inferred that the interface is axisymmetric on the average and the shape of the leading and trailing fronts are the same. The shape of the interface seems to be insensitive to changes in Re and x/D over the range of variables shown in the figure. Thus, it may be concluded that the velocity of the interface is constant across the pipe. The trailing front of a puff is quite similar to that of a slug. However, the leading front of a puff, which is rather vaguely defined, appears to be much more pointed. (See also Lindgren 1969.)

3.2. *The development of the laminar flow in the pipe*

One would like to specify precisely the nature of the flow which gives rise to puffs and slugs. This can be done in two ways: (i) by keeping Re and the inlet conditions constant and moving the sensors upstream to the location at which slugs or puffs originate and beyond; (ii) by keeping the hot wires at a given x/D

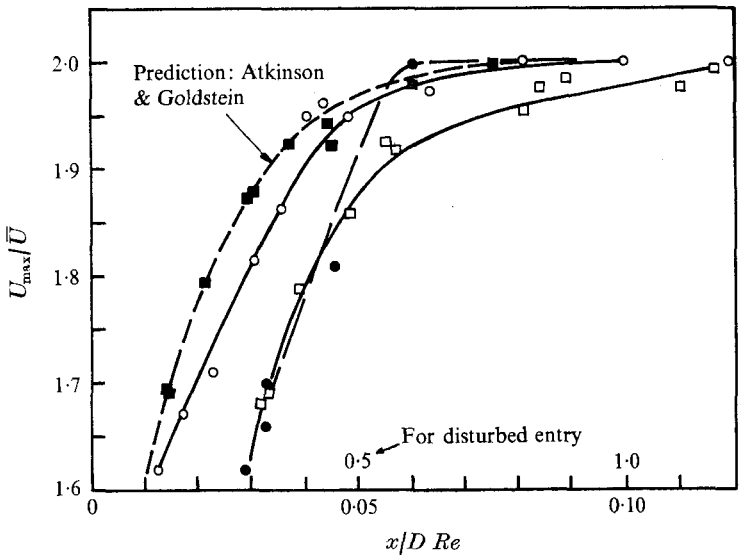

FIGURE 10. The dependence of the velocity at the centre of the pipe on $x/D\,Re$ for different conditions at the entrance. ○, $Re_T = 45 \times 10^3$, screen + honeycomb; □, $Re_T = 17{\cdot}5 \times 10^5$, honeycomb; ●, $Re_T = 2 \times 10^3$, disturbed entry; ■, Reshotko (1958).

and reducing Re to values which are equal to or smaller than Re_T. By doing both one could hope to estimate the effect of distance from the inlet and of Reynolds number separately, although the variables are not entirely independent of one another. We shall first examine the flow at a fixed distance from the inlet and describe the results from (i) in the next section.

Figures 9(*a*) and (*b*) show the dependence of the laminar velocity profile on Re at $x/D = 505$ for two different inlet conditions. The results in figure 9(*a*) were obtained with a honeycomb in the smaller settling chamber (figure 3) while the profiles in figure 9(*b*) were measured after a screen had been added immediately downstream of the honeycomb. At $x/D = 505$, the addition of a screen resulted in a change of Re_T from 17500 to 45000. For a small Re and thus large $x/D\,Re$, a parabolic profile was observed. A progressive increase in Re produced more bluntly defined velocity profiles. In the process the velocity distribution changed from a Poiseuille type to a typical laminar boundary-layer profile. Deviations from a parabolic profile took place long before any turbulence could be observed. The increase in Re not only resulted in a flatter velocity profile, but also increased the relative amplitude of low-frequency oscillations which were superimposed on the mean motion. It is generally believed that Poiseuille flow is stable to infinitesimal axisymmetric disturbances and this belief, although not proved, was certainly not violated in the course of the present investigation.

The inlet region of a pipe, in which the laminar flow is dependent on x, extends over several hundred pipe diameters. It is here that the velocity profile evolves from a uniform to a parabolic distribution. Theoretical calculations based on steady-state boundary-layer equations indicate that the evolution of the profile depends on a parameter $x/D\,Re$ (Goldstein 1938, p. 304; Christiansen & Lemmon

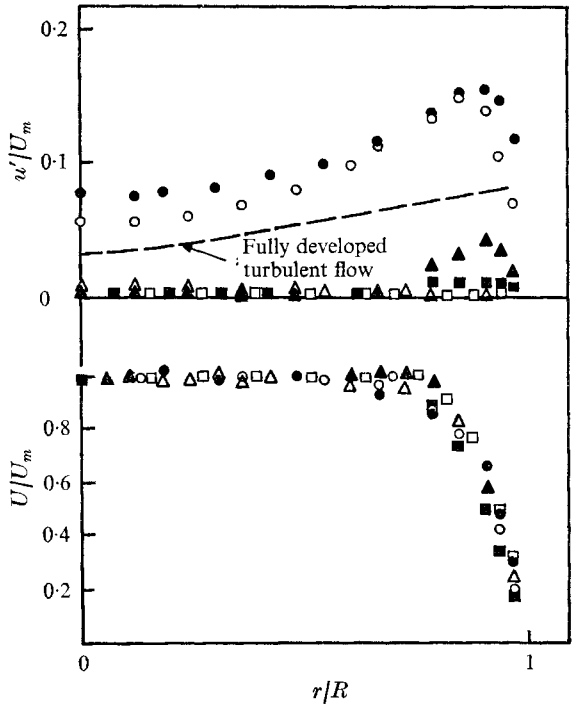

FIGURE 11. Mean velocity profiles and turbulent intensity distributions 15 diameters downstream of the inlet for various inlet conditions. Frequency = 2 c/s–10 kc. ●, honeycomb and orifice, Re = 2400 $(u'/U_m)_{\mathbb{C}}$ = 7·8%; ○, honeycomb and disk, Re = 2400, $(u'/U_m)_{\mathbb{C}}$ = 5·8%; △, honeycomb and cylinder, Re = 4200, $(u'/U_m)_{\mathbb{C}}$ = 0·36%; ▲, honeycomb only, Re = 19000, $(u'/U_m)_{\mathbb{C}}$ = 0·16%; ■, honeycomb only, Re = 10000, $(u'/U_m)_{\mathbb{C}}$ = 0·17%; □, honeycomb and screen, Re = 19000, $(u'/U_m)_{\mathbb{C}}$ = 0·14%.

1965). A comparison between figures 9(*a*) and (*b*) shows that $x/D\,Re$ does not uniquely determine the shape of the velocity profile. In figure 10 the velocity $U_{\max}$ at the centre is plotted versus $x/D\,Re$. Whenever $U_{\max}/\overline{U} = 2$, the parabolic profile was attained, which implies that the pipe flow became fully developed. Four different cases are presented in the figure. The first two were mentioned earlier in conjunction with figures 9(*a*) and (*b*). The third case represents an orifice plate at the entrance and the fourth shows measurements made by Reshotko (1958). The results did not collapse onto a single curve. The most significant deviation resulted when the flow at the entrance was artificially disturbed. (The abscissa is an order of magnitude larger in this case.) One may think that the comparison is invalid because the velocity distribution near the inlet is not uniform. For all three cases under investigation, however, the velocity profiles at x/D = 15 were almost identical (figure 11). Thus, the differences shown in figure 10 cannot be attributed to initial differences in the mean motion.

The length of the inlet region depends not only on $x/D\,Re$, but also on the nature of the input disturbances. The simplest additional parameter for characterizing the nature of the input disturbances is the transition Reynolds number. One

may approximately collapse the curves in figure 10 onto the curve for $Re_T = 45\,000$ by multiplying $x/D\,Re$ by $Re_T/45\,000$, i.e. the ratio of the transition Reynolds numbers. In fact, the families of velocity profiles shown in figures 9(*a*) and (*b*) can be collapsed onto one curve by multiplying the values of $x/D\,Re$ in figure 9(*a*) by 17·5/45. The data for $Re_T = 45\,000$ (figure 10) are close to Reshotko's results, which were obtained with nearly ideal inlet conditions, and agree with theoretical predictions which are valid in the limit for which input disturbances vanish.

We think that the bluntness of the velocity profiles can be attributed in part to Reynolds stresses which exist in the flow, although it is ostensibly laminar. The initial Reynolds stresses must be particularly high whenever the pipe is purposely disturbed. Thus, for practical purposes, the inlet region should not only be regarded as the length required for the wall boundary layers to join, but also as the length necessary to dampen the entering disturbances. The partial failure of the theoretical analyses (Goldstein 1938, p. 304) stems from considering the steady-state equations of motion. It is significant that never throughout the present investigation were slugs observed while the velocity profile was close to parabolic. Thus, stability calculations in the developing region of the pipe (Tatsumi 1952) are more relevant to the natural process of transition in a pipe than the numerous analyses which are solely concerned with the stability of Poiseuille flow.

3.3. *Conditions near the entrance and the origin of slugs and puffs*

Moving the sensors close to the entrance provided some insight into the distinction between puffs and slugs. In the bottom part of figure 11, velocity profiles obtained at $x/D = 15$ for a variety of inlet conditions are shown. The normalized radial distributions of the mean axial velocity are not very sensitive to disturbances at the inlet. Thus, the mean flow adapts itself quickly to the local boundary condition as it does in many turbulent shear flows. On the other hand, the level of the longitudinal fluctuations rises abruptly once the obstruction at the inlet exceeds a given size. As long as the perturbation at the inlet is small and $Re < Re_T$ the fluctuation level 15 diameters downstream is a fraction of a per cent of the mean velocity. When Re approaches Re_T, as in the case of the honeycomb at $Re = 19\,000$, the amplitude of the fluctuations increases in the vicinity of the wall and may eventually burst into turbulence. The growth of the perturbations is associated with the large mean shear existing within the boundary layer.

Whenever the flow entering the pipe is disturbed beyond a given level, the entire region in the neighbourhood of the inlet becomes turbulent. In the vicinity of the fixed obstruction the level of turbulence exceeds the level in a fully developed turbulent pipe flow. Since the mean motion in the pipe cannot sustain such a high level of turbulence, an adjustment must take place. It is interesting to note that the maximum level of the longitudinal component u'/U of the disturbance is about 0·16, comparable with the level required in order to trigger a turbulent spot in a boundary layer over a flat plate (Elder 1960). At the transitional Reynolds number the turbulent region extends some 30 diameters downstream from the inlet. Further downstream the flow becomes intermittent as smaller chunks of turbulence break away and move downstream. The process of subdivision may

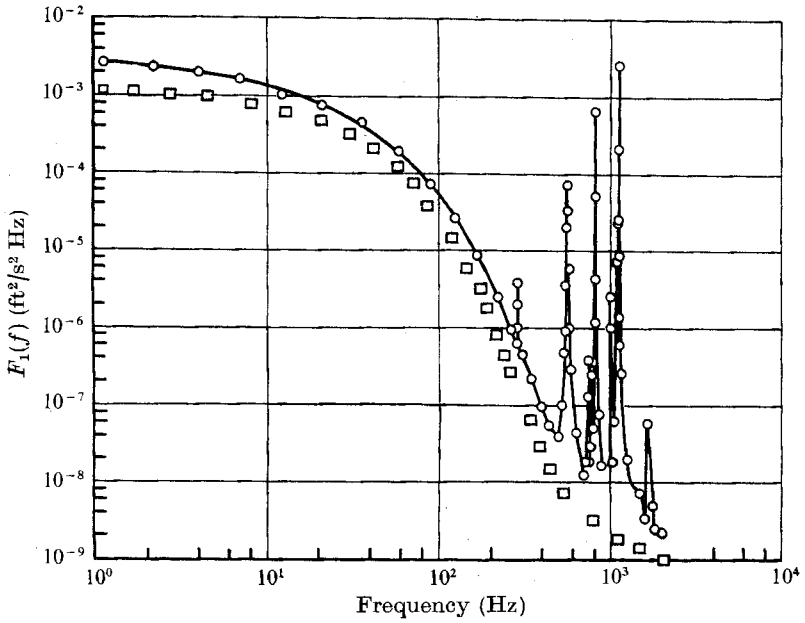

FIGURE 13. Narrow-band spectra for two different inlet disturbances. $x/D = 15$, $r = 0$, $Re = 2400$. ○, orifice; □, disk.

repeat itself until an equilibrium is reached and 'fully developed' puffs move down the pipe.

The breakdown of the turbulent region downstream from the inlet was observed by looking at hot-wire traces as well as by conventional flow visualization. Figure 12 (plate 3) comprises four photographs, two of which were taken just after dye was injected upstream of an orifice plate, and the other two while a suspension of pearlessence in water was circulating in the system. The pipe was illuminated in a plane containing the centre and perpendicular to the line of sight of the observer. Near the entrance the dye mixed violently and filled the entire cross-section of the pipe. A short distance downstream ($x/D \approx 30$) the dye filaments were stretched in the axial direction with no apparent transverse motion. The leading and trailing fronts of a puff are shown in the lower photographs. Near the trailing front, one may see that the pearlessence is agitated (the degree of agitation is related to the level of turbulence), in particular at the central portion of the pipe. Very little agitation is visible near the leading edge, which cannot be clearly identified.

We have seen (figure 11) that different levels of turbulence are associated with different obstructions at the inlet, and yet the flow in the fully developed puff was independent of the original disturbance, as we shall see later. We wondered whether the geometry of the pipe exerted major influence on the puff or whether all the obstructions which were introduced to the inlet produced turbulent flow of similar structure even though the initial levels were different. In order to resolve this question, narrow-band spectra were measured 15 diameters downstream of two different obstructions, a disk and an orifice plate, and the results

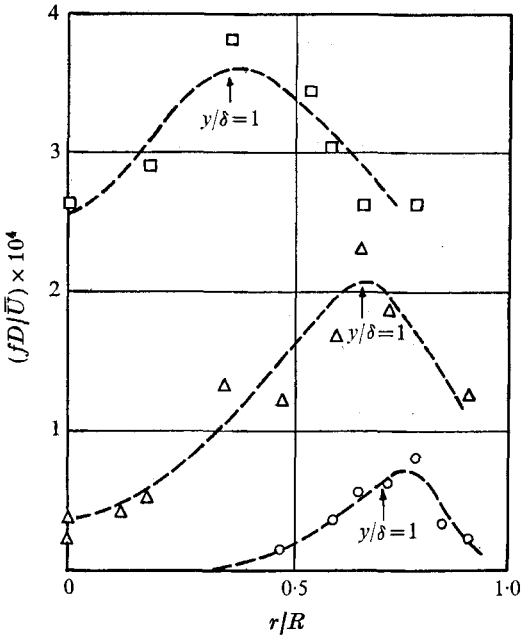

FIGURE 15. Radial distribution of the frequency of turbulent spots and slugs at various distances from the pipe inlet. ($y/\delta = 1$ represents the outer edge of boundary layer defined in a conventional way.) $Re = 3{\cdot}5 \times 10^4$. ○, $x/D = 20$; △, $x/D = 30$; □, $x/D = 40$.

are shown in figure 13. Turbulence produced by the orifice contained strong discrete and orderly structure which is probably related to vortex rings being shed at the orifice (e.g. Crow & Champagne 1971). In contrast, the spectral distribution of the longitudinal fluctuations produced by a disk contained no peaks. The structure of the flow within a fully developed puff thus appears to be independent of the original turbulent structure existing in the inlet region, the region which gave rise to the puff in the first place.

We shall now turn our attention to the origin of turbulent slugs. So far as we know that they do not originate at the entrance itself (figure 11), because the turbulence level measured near the entrance was very low. Yet their origin is associated with the inlet region since the laminar flow was never fully developed as Re approached Re_T. We have also seen that some perturbations amplify near the wall. Slugs seem to be a product of transition in the developing boundary layer downstream of the entrance. Figure 14 (plate 4) is a collection of oscilloscope traces showing how a boundary-layer spot begins on one side of the pipe wall and grows into a slug as its dimensions become comparable with the pipe diameter. A dual-beam oscilloscope was used and the two traces in each photograph represent the simultaneous outputs from two hot wires, located diametrically opposite one another, but at the same radial distance from the centre-line. The lowest photograph in this figure shows a spike in the velocity a short time after a burst into turbulence on one side of the pipe occurred. The flow at the opposite radial location was hardly disturbed, although one can notice a small disturbance which was probably communicated there by a pressure wave. In the central

photograph a larger turbulent region (spanning more time) is shown and its effect on the flow across the centre-line is stronger. In the uppermost photograph turbulent flow of short duration occurred across the entire pipe. It may be deduced that the breakdown to turbulence is a local phenomenon which is independent of the axial symmetry of the pipe and does not occur instantaneously across the entire cross-section. Some quantitative information is given in figure 15. The local boundary-layer thickness, at $y/\delta = 1$, is shown by an arrow at three discrete distances from the inlet. It was determined in the conventional way based on mean velocity profiles. The radial distribution of the frequency of occurrence of turbulence is also shown on the same plot. At $x/D = 20$ (and $Re = 3{\cdot}5 \times 10^4$) no turbulence could be detected in the central core of the pipe, and since $\delta \approx \frac{1}{4}R$, one can expect that a turbulent burst occurring within this boundary layer should resemble the classical Emmon's spot. The observation of turbulence at $y/\delta > 1$ is not at all surprising because δ is a long-time average thickness and a turbulent spot usually extends beyond it (Schubauer & Klebanoff 1956).

At $x/D = 30$, some slugs were already visible and at $x/D = 40$ about 75 % of the turbulent bursts detected encompassed the entire cross-section of the pipe. The largest number of turbulent bursts or sudden strong spikes in the velocity occurred near the outer part of the boundary layer. The local velocity spikes are characteristic of regions of concentrated vorticity, which occur prior to a complete breakdown to turbulence. Similar spikes were observed by Kovasznay *et al.* (1962). They increase in amplitude until they exceed a threshold level and then burst into turbulent spots (see also Elder 1960). When the spots are small they are localized in the boundary layer where they originated (figure 15). They occur randomly in time and azimuthal location in the pipe. Turbulent spots could only be observed when the parameter $x/D\,Re$ was very small (i.e. $x/D\,Re \approx 10^{-4}$), and hence the flow was far from being 'fully developed'. At larger values of $x/D\,Re$ slugs exclusively represented the occurrence of turbulence. This is quite understandable because at larger $x/D\,Re$ the thickness of the boundary layer is comparable with R and a burst occurring at one point near the centre of the pipe (at $y/\delta \approx 1$) is almost instantaneously communicated across the entire cross-section.

3.4. *The structure of fully developed pipe flow and the interior of a turbulent slug*

We have discussed in § 3.2 the behaviour of the laminar flow in the pipe and the effect of Re on the flow. Having discussed the state of the pipe flow at low Reynolds numbers, we shall describe the evolution of the slugs into fully developed pipe turbulence with increasing Reynolds number. Detailed measurements in the fully developed turbulent pipe flow were made by Laufer (1954). The pipe in Laufer's experiment was approximately 10 in. in diameter and 40 ft long. The boundary-layer growth was artificially accelerated by roughening the surface near the entrance. Since the present apparatus was quite different we felt that more confidence in the universality of our results would be derived if we were to repeat some measurements in the fully turbulent pipe flow at Laufer's Reynolds number of 5×10^4. We also wanted to appraise the effects of lowering the value

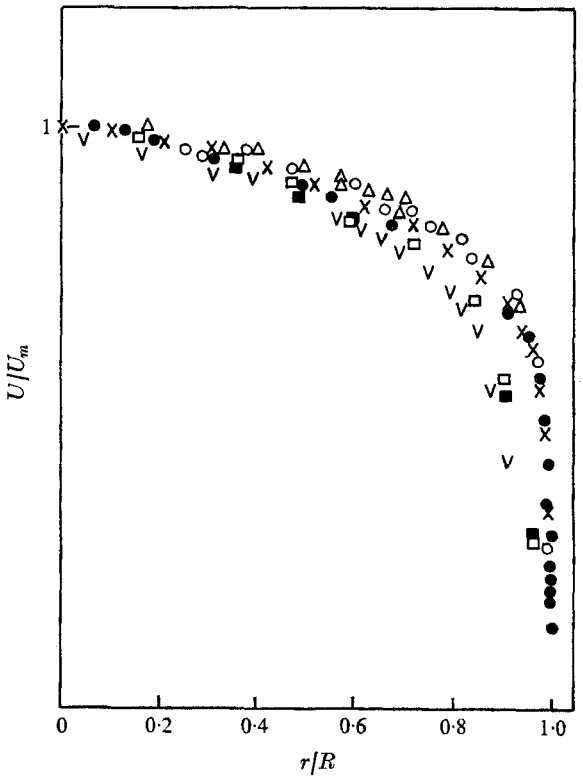

FIGURE 16. Mean velocity distribution in fully developed pipe flow and in the interior of turbulent slugs.

	Fully turbulent			Transitional flow		
	$Re \times 10^{-4}$			$Re \times 10^{-4}$	$(X_{LE}/D)_{\text{¢}}$	(X_{TE}/D)
×	5	Laufer (1954)	□	0·4	−20	—
●	5	Present results	■	0·4	—	20
V	0·8	Wygnanski (1971)	○	1·9	−20	—
			△	1·9	—	20

of Re below those at which data are available to compare the flow in a fully turbulent pipe with the flow in a slug.

A group of mean velocity profiles normalized with the centre-line velocity U_m is illustrated in figure 16. The measurements made in fully turbulent flow at $Re = 5 \times 10^4$ agree very well with those of Laufer. The effect of lowering Re can be estimated by comparison with a previously obtained velocity distribution at $Re = 8 \times 10^3$ which was measured in a 2 in. pipe (Wygnanski 1971). The ensemble-averaged velocity profiles in the interior of turbulent slugs are somewhat more blunt than the velocity distribution in a fully turbulent flow at a comparable Re. The difference, however, is small and it may be attributed to experimental error. The location chosen to represent the interior of a slug was 20 diameters removed from either the leading or trailing interface. (X_{LE} denotes distance from the leading front; it is positive in the direction of the mean flow. The subscript ¢ means that the distance was measured from the

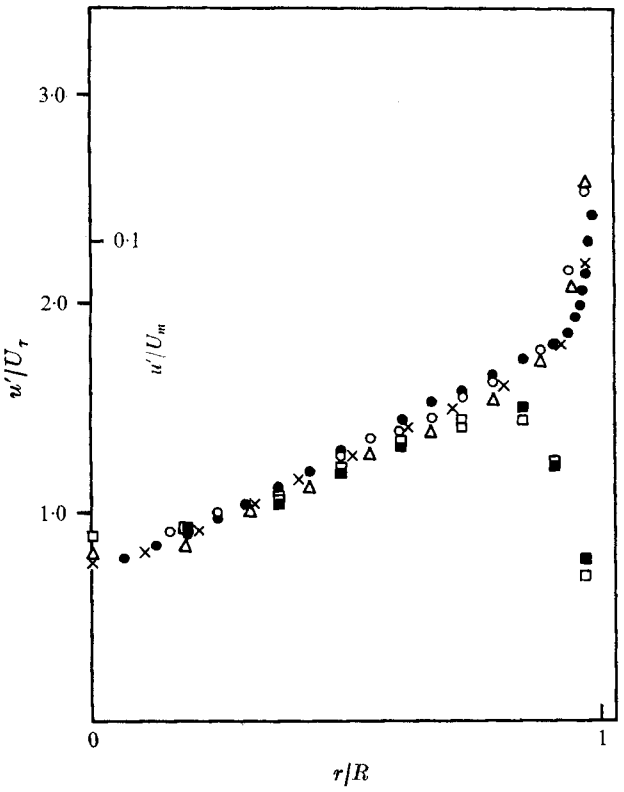

FIGURE 17. The distribution of u' in the interior of a slug and in fully turbulent flow.

Fully developed turbulent pipe flow

$Re \times 10^{-4}$				$Re \times 10^{-4}$	$(X_{LE}/D)_{\mathbb{C}}$	$(X_{TE}/D)_{\mathbb{C}}$
×	5	Laufer (1954)	○	1·9	−20	—
●	5	Present results	△	1·9	—	20
			□	0·42	−20	—
			■	0·42	—	20

average location of the front on the centre-line. X_{TE} denotes the distance from the trailing front. See figure 3 (*b*) for notation.) In a previous investigation (Wygnanski 1971) turbulent zone-average measurements were obtained; here, this procedure was avoided because it was felt that by incorporating the regions near the interface in the averaging process one might distort the results.

The three components u', v' and w' of the velocity fluctuations and the turbulent shear stress $\overline{uv}$ are shown in figures 17–20. The data were also normalized by U_τ, the friction velocity. The level and distribution of all the components of the fluctuations in fully turbulent flow at $Re = 5 \times 10^4$ are in agreement with those in the interior of the slugs at $Re = 1{\cdot}9 \times 10^4$. The radial distribution of the velocity fluctuations in the interior of a slug at $Re = 0{\cdot}42 \times 10^4$ is different from that in all other cases. The disparity is particularly obvious in figure 17, in which the longitudinal fluctuations are shown. The disparity can be attributed

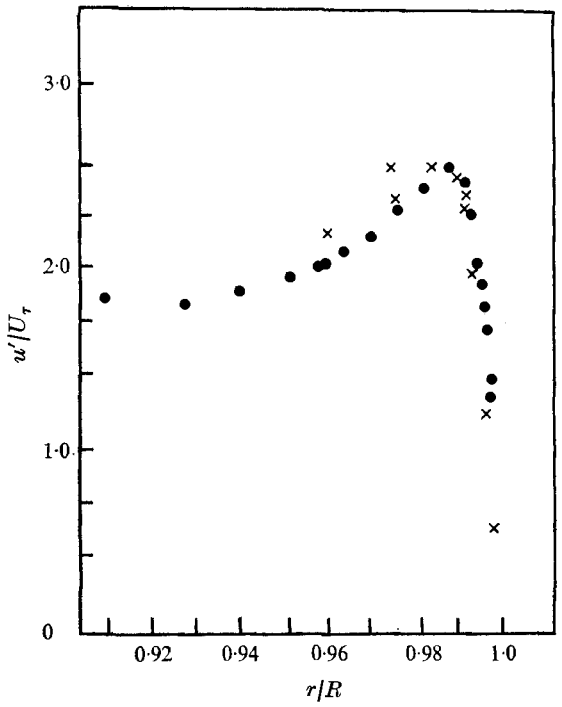

FIGURE 18. The distribution of u' near the wall; a comparison with Laufer's measurements. $Re = 5 \times 10^4$; ×, Laufer (1954); ●, present results.

to the low Reynolds number. The comparison is somewhat similar to that made by Laufer in fully turbulent flow between $Re = 5 \times 10^4$ and $Re = 5 \times 10^5$. At the lower Re the effects of the predominantly viscous layer near the wall are magnified. The effect of Re on the turbulent intensity at the centre of the pipe is negligible over the range considered. The agreement between the current measurements of u' and those of Laufer is very good even in the vicinity of the wall (figure 18). The level of the radial and azimuthal fluctuations in fully turbulent flow differs slightly from the level measured by Laufer and agrees better with measurements of Patel (1968) at $Re = 2 \times 10^5$ in the central region of the pipe. The level of these fluctuations in the interior of a turbulent slug is somewhat higher than in fully turbulent flow, particularly at low Re. This difference is attributed to data being obtained at an insufficient distance from the interface of the slug. As we shall see later, there is enhanced turbulent activity near the interface and a distance of 20 diameters might have been inadequate.

An attempt was made to measure the pressure jump across the interface by embedding a small Bytrex pressure transducer in the surface of the pipe and processing its output through the wave-form eductor in a manner described previously. The ensemble-averaged time record of the transducer is shown in the lower part of figure 21. The abscissa was rendered dimensionless by multiplying the time by the velocity of the leading front and dividing through by the distance between the transducer and the exit of the pipe. The ordinate was left in dimensional form. The choice of the particular parameters was made because the

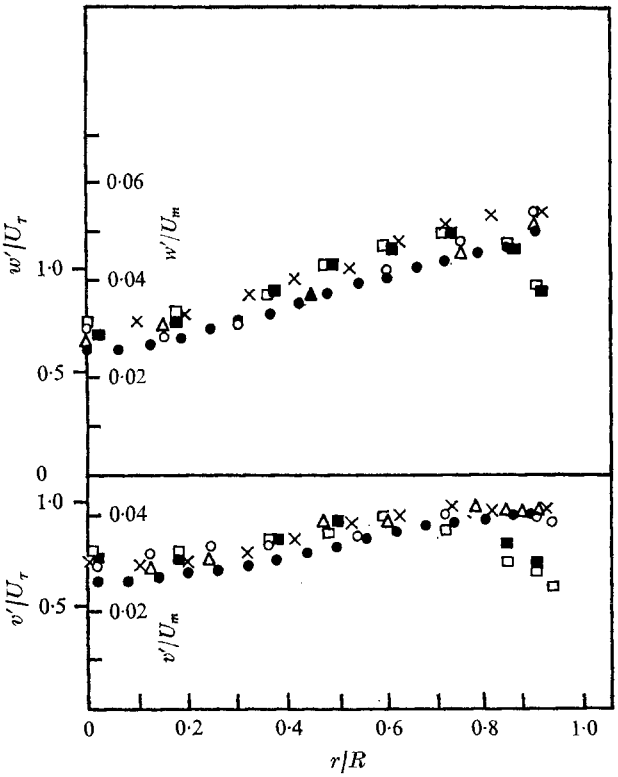

FIGURE 19. The distribution of v' and w' in the interior of a slug and in fully turbulent pipe flow. Symbols as in figure 17.

transducer was referenced to atmospheric pressure. Thus, when

$$TU_{LE}/(x_{\text{trans}}-x_{\text{exit}}) \begin{cases} = 0 & \text{the leading interface is at the transducer,} \\ < 0 & \text{only laminar flow exists between the transducer and the exit since } \gamma \text{ was small,} \\ = 1 & \text{the leading interface was just dislodged from the exit of the pipe,} \\ > 1 & \text{only turbulent flow separates the transducer from the atmospheric pressure at the exit,} \end{cases}$$

where x_{trans} denotes the location of the transducer.

As the resolution from the pressure transducer was ± 5 ms (caused by low-pass filtering at 50 Hz), the above definitions are necessarily not exact with regard to what portion of the interface is referred to. The length of the interface is equivalent to a $TU_{LE}/(x_{\text{trans}}-x_{\text{exit}})$ of about 0·1.

If a discontinuity in pressure were to exist across the leading interface it would show on figure 21 as two horizontal lines at different levels of constant pressure for values of $TU_{LE}/(x_{\text{trans}}-x_{\text{exit}}) < 0$ and $TU_{LE}/(x_{\text{trans}}-x_{\text{exit}}) > 1$, which are joined by an inclined straight line extending between

$$0 \leqslant [TU_{LE}/(x_{\text{trans}}-x_{\text{exit}})] \leqslant 1.$$

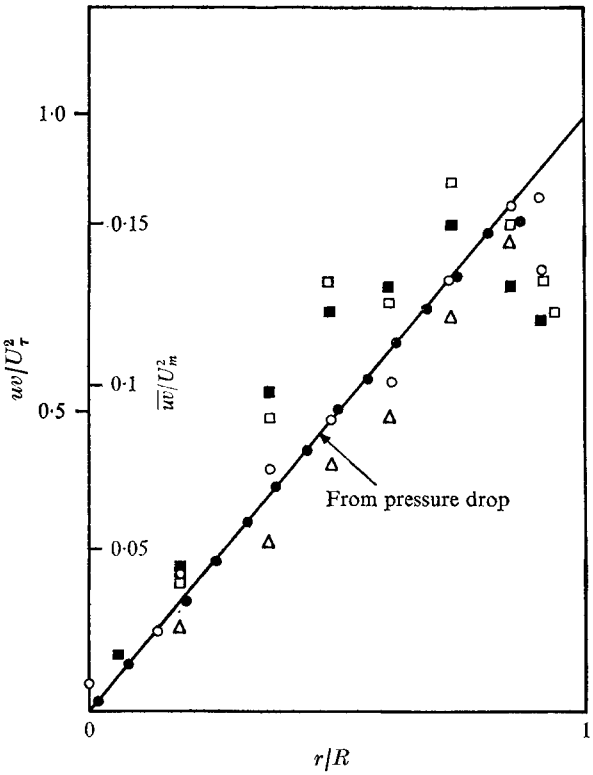

FIGURE 20. The turbulent shear stress in the interior of a slug and a fully turbulent pipe flow. Symbols as in figure 17.

The ensemble-averaged pressure record shows that the general trend is in agreement with the above mentioned description. The rounded junctures might have been caused by small variations in the velocity and shape of the leading interfaces and by the time response of the transducer. The average pressure drop resulting from the flow in the laminar and turbulent regions may be obtained from this figure. The upper left part of figure 21 shows a momentum balance for the laminar flow existing 10 pipe diameters in advance of a leading front of a turbulent slug. Comparison of succeeding velocity profiles indicated that inertia terms are negligible although we know that the laminar flow was not fully developed. The radial distribution of the viscous terms is shown by discrete dots on the figure and when the curve is extrapolated to the wall it agrees with the measured pressure drop. If the laminar velocity profiles had been parabolic the pressure drop occurring in the pipe for the same average mass flow should have been one-third as large. The viscous terms are very much smaller in the central core of the pipe because the laminar velocity profile is rather blunt. By assuming that the pressure is constant across the pipe one can calculate the Reynolds stresses which exist in this perturbed laminar flow. Those stresses have to vanish at the wall as they indeed do. In the upper right part of figure 21 a comparison is made between $\overline{uv}$ in the laminar and turbulent portions of the flow excluding the regions immediately adjacent to the interface. On the average, the $\overline{uv}$ correlation

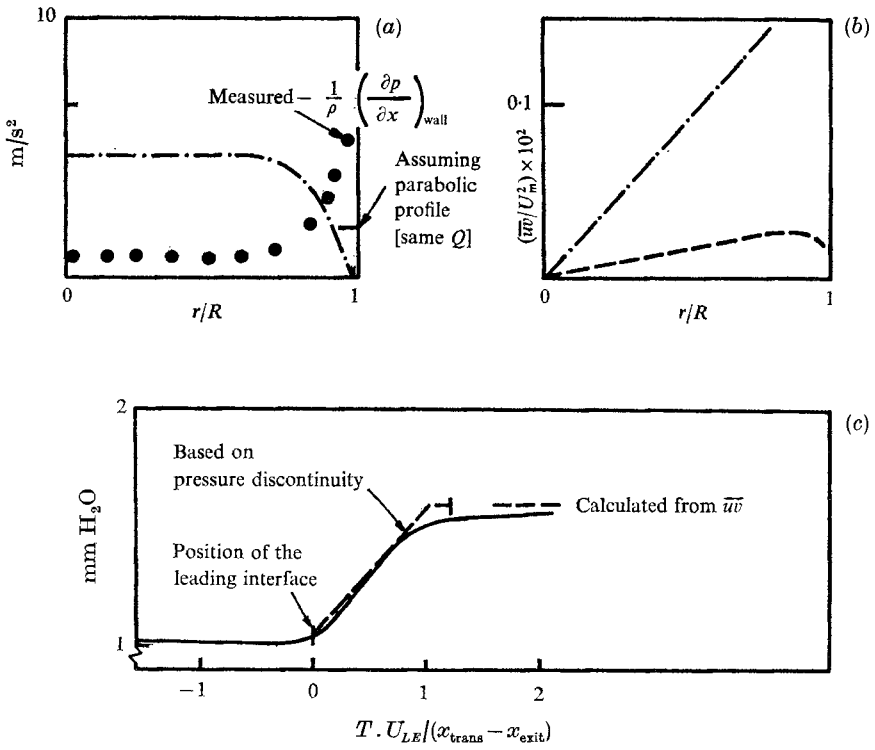

FIGURE 21. (*a*) Momentum balance in the laminar region; (*b*) comparison of Reynolds stresses in the laminar and turbulent zones; and (*c*) ensemble average of static pressure recordings near the leading interface of a slug. (*a*) $(X_{LE}/D)_{\mathbb{Q}} = 10$; –·–·, $r^{-1}[\partial ruv/\partial r]_{lam}$; ●, $\nu\nabla^2 U$. (*b*) $(X_{LE}/D)_{\mathbb{Q}}$: –·–·, –20 (turbulent); – – –, 10 (laminar).

in the turbulent region is five times larger than that in the laminar region, but the latter is not negligible. There is, of course, a large difference in the frequencies involved.

The ordinates in figures 17–20 and 22 were rendered dimensionless by dividing through by either the velocity U_m at the centre or the shear stress velocity U_τ. The latter was derived in a conventional manner from the pressure record shown in figure 21. In order to make our comparison between the fully developed turbulent pipe flow and the flow in the slug more complete, measurements related to the dissipation rate were made. One such measurement of $\overline{(\partial u/\partial x)^2}$ is shown in figure 22. The spatial derivative with respect to x was obtained from a temporal derivative using Taylor's transformation. First, our measured $\overline{(\partial u/\partial x)^2}$ was compared with Laufer's data at $Re = 5\times 10^4$; the agreement between the two sets of measurements is good, particularly in the central region of the pipe. Since one does not expect Reynolds number similarity for the viscous dissipation terms, the entire measurement was repeated for fully turbulent pipe flow at $Re = 1{\cdot}9\times 10^4$. The fully turbulent flow at $Re = 1{\cdot}9\times 10^4$ was obtained by slightly disturbing the flow at the inlet. The ratio of the magnitudes of $\overline{(\partial u/\partial x)^2}$ at the two values of Re is approximately proportional to the ratio of the values of Re at which the

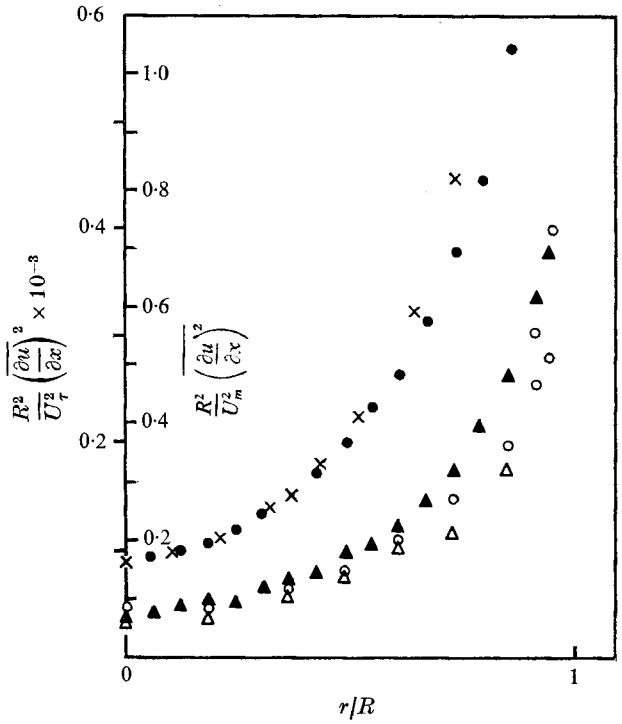

FIGURE 22. A comparison between $\overline{(\partial u/\partial x)^2}$ measured in the interior of a slug and in fully developed turbulent pipe flow and the effect of Re on this term. ▲, fully turbulent flow, present results at $Re = 1{\cdot}9 \times 10^4$. Other symbols as in figure 17.

measurements were carried out. Measurements in the interior of the slug coincide with the measurements in the fully turbulent pipe flow at the same Re.

From the results presented we may conclude that the flow in the interior of the turbulent slug is identical to the fully developed turbulent pipe flow. Some third-order terms were also measured and a comparison was made between the results obtained in a slug and the results obtained in a fully turbulent flow. The agreement was again good. The results are not shown. The rate of turbulent energy production at a point is approximately balanced by the rate of energy dissipation throughout the cross-section, with the exception of a small central core. Turbulent diffusion is thus relatively unimportant. Because of the strong turbulent activity near the interface, a length of approximately 20 diameters had to be excluded at each end from the comparison. Sometimes one may observe on an oscilloscope a region of high turbulence activity in the middle of a slug. This occurs whenever the point of observation is a small distance downstream of a point at which a leading front of a slug caught up with the trailing front of the preceding slug. The occurrence of this phenomenon and its ensuing effects can be eliminated by making the measurements at a Re for which γ is small.

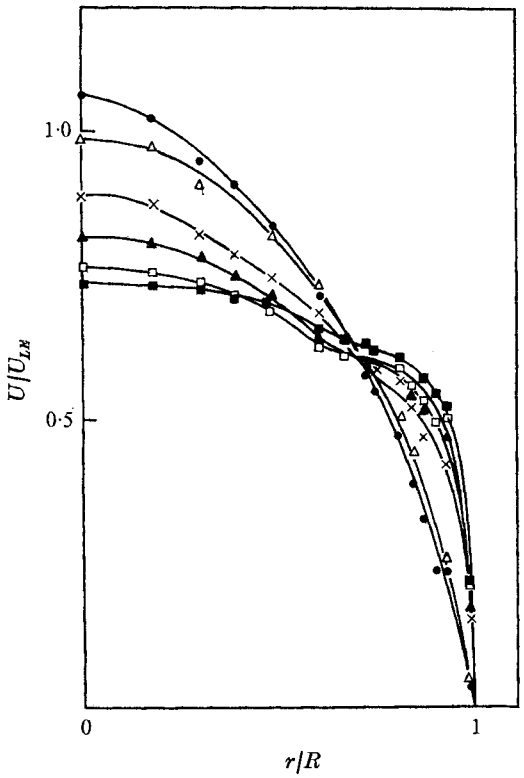

FIGURE 23. Ensemble-averaged velocity profiles near the leading interface. $Re = 1{\cdot}9 \times 10^4$, $x/D = 505$, $U_{LE}/\bar{U} = 1{\cdot}5$.

	●	△	×	▲	□	■
$(X_{LE}/D)_{\mathbb{C}}$	+3·75	−3·00	−6·74	−8·63	−10·5	−18·0

3.5. *The motion near the interface of a slug*

So far we have discussed some properties of the flow in the interior of a slug which occupies over 90 % of the length of a typical slug at $x/D \approx 500$. Yet the most interesting flow phenomena occur in the vicinity of the interface where laminar fluid is entrained into the turbulent region. In figures 23 and 24 ensemble-averaged velocity profiles measured near the leading and trailing fronts are shown. A turbulence detector was embedded in the surface of the pipe one metre upstream of the measuring station. Whenever an interface was detected a triggering pulse initiated the acquisition of data at the measuring station. We refer to the average distance measured along the centre-line of the pipe from the leading and trailing edges as $(X_{LE})_{\mathbb{C}}$ and $(X_{TE})_{\mathbb{C}}$ respectively (see figure 3*b*). The distances were obtained from temporal records and knowledge of the propagation velocity of a given interface.

In figure 23, we can follow the changes in velocity as we proceed in our discussion from the laminar region upstream of the interface to the turbulent region downstream of it. The first profile shown at $(X_{LE}/D)_{\mathbb{C}} = 3{\cdot}75$ was measured entirely downstream of the interface. It resembles a laminar boundary-layer

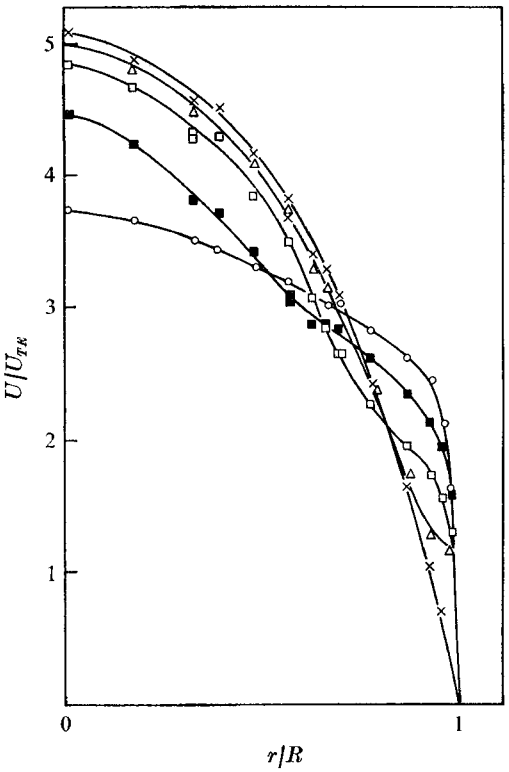

FIGURE 24. Ensemble-averaged velocity profiles near the trailing interface. $Re = 1{\cdot}9 \times 10^4$, $x/D = 505$, $U_{TE}/\overline{U} = 0{\cdot}35$.

	×	△	□	■	○
$(X_{TE}/D)_{\mathbb{C}}$	−3·88	−0·43	2·15	4·74	8·18

profile and is similar to the laminar profiles which were measured in the pipe at $Re < Re_T$. The next profile at $(X_{LE}/D)_{\mathbb{C}} = -3$ was taken almost entirely inside the turbulent region. (The interface is slightly more than three diameters long, see figure 8.) Over the intervening distance the flow on the axis of the pipe decelerates by approximately 5 %. There is no discontinuity in the velocity across the interface as might have been inferred by a cursory look at the oscillogram in figure 4 (plate 1). The deceleration on the axis of the pipe increases initially with increasing distance from the interface and reaches a maximum when $(X_{LE}/D)_{\mathbb{C}} = -6$. Since the volume flow in the pipe is constant a deceleration in the central region of the flow must be accompanied by a corresponding acceleration near the wall. A single radial location ($r/R \approx \frac{2}{3}$) separates the fluid undergoing acceleration from the decelerating fluid. About 6 diameters away from the leading interface the velocity profile develops a strong inflexion point. The inflexion point is recognizable at $-20 \leqslant (X_{LE}/D)_{\mathbb{C}} \leqslant -5$. The slope of the velocity profile at the wall increases rapidly after the passage of the interface and with it the shear stress and the accompanying pressure drop must also increase.

The fluid entering the slug from the rear also undergoes a deceleration in the

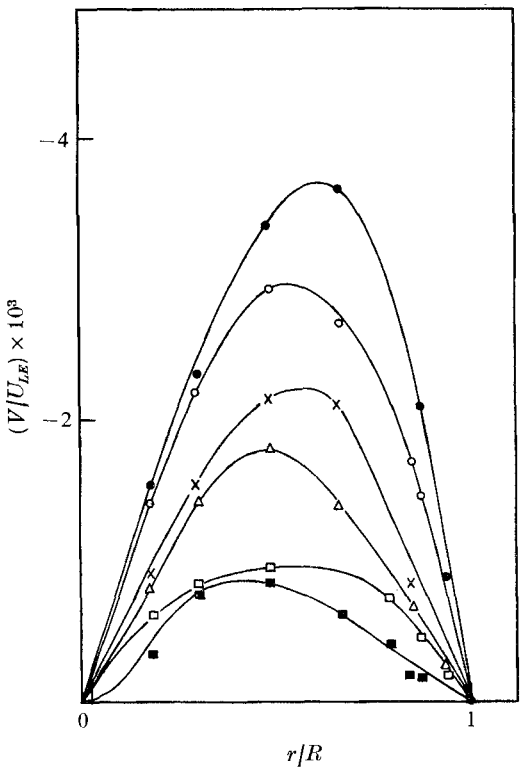

FIGURE 25. A calculated radial velocity distribution near the leading interface. $Re = 1{\cdot}9 \times 10^4$, $x/D = 505$, $U_{LE}/\bar{U} = 1{\cdot}5$.

$(X_{LE}/D)_{\mathbb{Q}}$	□	×	●	○	△	■
	−1·12	−3·00	−6·75	−8·62	−10·50	−12·35

central portion of the pipe and an acceleration near the wall (figure 24). Nevertheless, the process is different from that near the leading front. The strongest acceleration occurs in the immediate neighbourhood of the wall right at the interface. For example, the velocity profile at $(X_{TE}/D)_{\mathbb{Q}} = -0{\cdot}43$ has an inflexion point at $r/R > 0{\cdot}9$. The inflexion point moves towards the centre with increasing distance into the core of the slug. The strength of the inflexion erodes in the process, and the inflexion disappears before $(X_{TE}/D)_{\mathbb{Q}} = 8$.

The radial velocity V was computed from figures 23 and 24 and is shown in figures 25 and 26. This velocity is far too small to be measured with an X-wire, so the points shown in the figures were computed from $\partial U/\partial x$. The maximum radial velocity calculated is approximately 1 % of the maximum velocity in the interior of the slug. Near the leading interface, V peaks around $r/R \approx 0{\cdot}5$ almost independently of X_{LE}. The radial position at which V has a maximum near the trailing interface, on the contrary, moves from $r/R \approx 0{\cdot}8$ to $r/R \approx 0{\cdot}4$ with increasing distance into the slug.

In an attempt to provide an explanation for the seemingly different behaviour of the mean motion near the leading and trailing fronts, we recomputed the velocity distributions in a frame moving with the relevant interface. The length

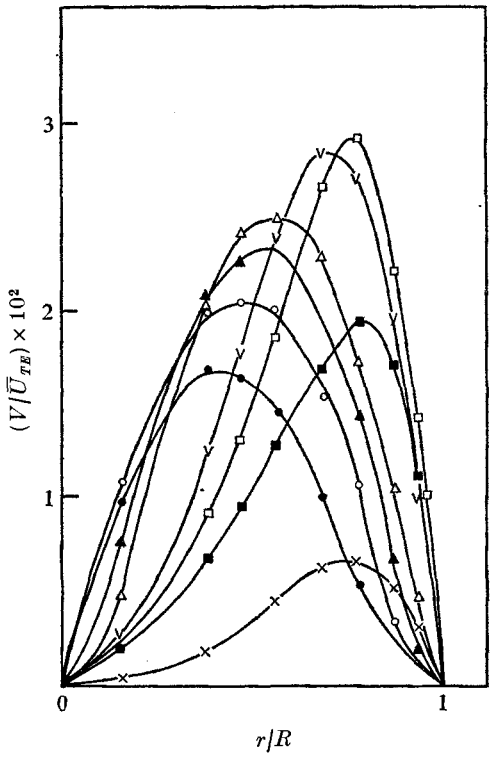

FIGURE 26. A calculated radial velocity distribution near the trailing interface. $Re = 1{\cdot}9 \times 10^4$, $x/D = 505$, $U_{TE}/\overline{U} = 0{\cdot}35$.

$(X_{TE}/D)_{\mathbb{C}}$	×	■	□	V	△	▲	○	●
	−0·43	0·43	1·29	2·15	3·01	3·87	4·73	5·6

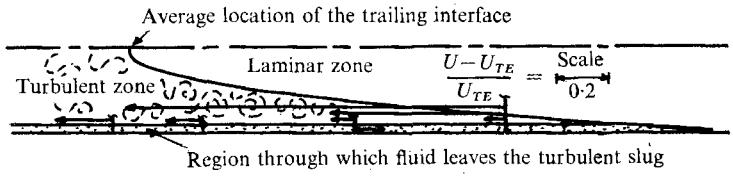

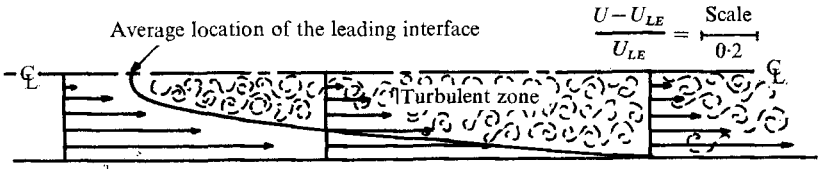

FIGURE 27. Velocity vectors relative to the leading and trailing interfaces (the average shape of the interfaces is drawn to scale). $Re = 1{\cdot}9 \times 10^4$, $x/D = 505$, $U_{LE}/\overline{U} = 1{\cdot}5$, $U_{TE}/\overline{U} = 0{\cdot}35$.

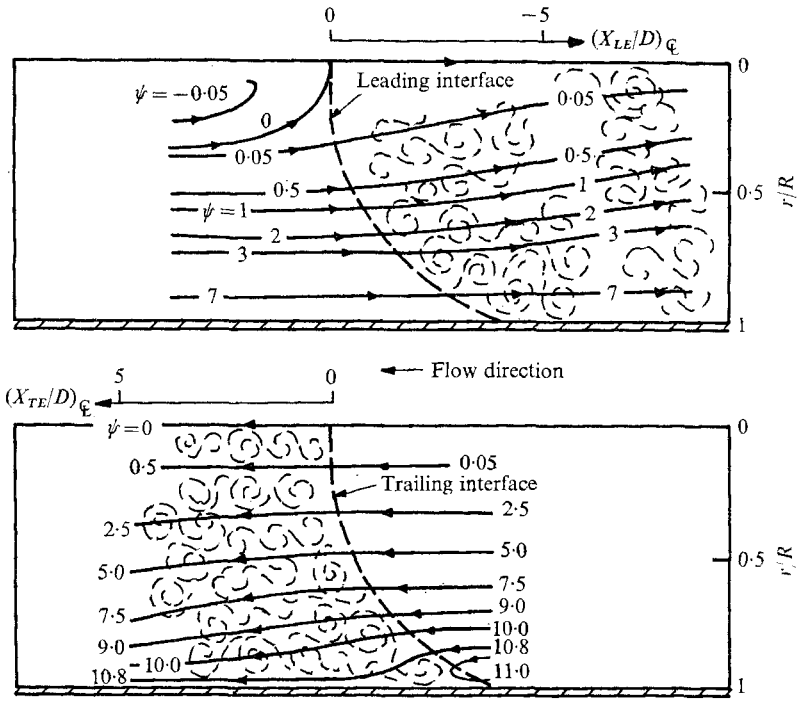

FIGURE 28. The streamline pattern relative to the leading and trailing fronts. $Re = 1{\cdot}9 \times 10^4$, $x/D = 505$.

and direction of the arrows in figure 27 correspond to the velocity vectors relative to the interface. The origin of each arrow is representative of its location in relation to an average interface which is also drawn to scale in the figure. It transpires that *the leading interface moves with a speed which is equal to the maximum velocity in the laminar region preceding it.* Thus, the velocity relative to the leading interface varies from zero at the centre of the pipe to $-U_{LE}$ at the wall, U_{LE} being the speed of the leading edge. In this manner no relaminarization of turbulent fluid can occur near the leading edge.

Since the trailing interface moves at a velocity U_{TE} which is independent of the radial location, it must overtake some fluid in the vicinity of the wall which moves slower than U_{TE} owing to the no-slip condition at a solid boundary. As a result of the rapid acceleration of the entrained flow as it crosses the interface at large r, the region from which fluid can escape from the slug is limited to a very narrow strip near the solid surface. One may suggest, after examining figure 27, that the fluid leaving the slug lies within the viscous sublayer. Experimental evidence lends credence to this notion because some 15 diameters away from the interface, the velocity distribution obeys a universal logarithmic law down to a distance from the wall equal to $yU_\tau/\nu \approx 30$, at which point $U/U_\tau \approx 15$. But $U_{TE}/U = 1$, corresponding to $U_{TE}/U_\tau \approx 6$, occurs at $yU_\tau/\nu \approx 6$ and is considered to lie within the viscous sublayer. The comparison can not be made closer to the interface because the velocity distribution is no longer universal. However, the conditions near the interface are even more favourable for the existence of

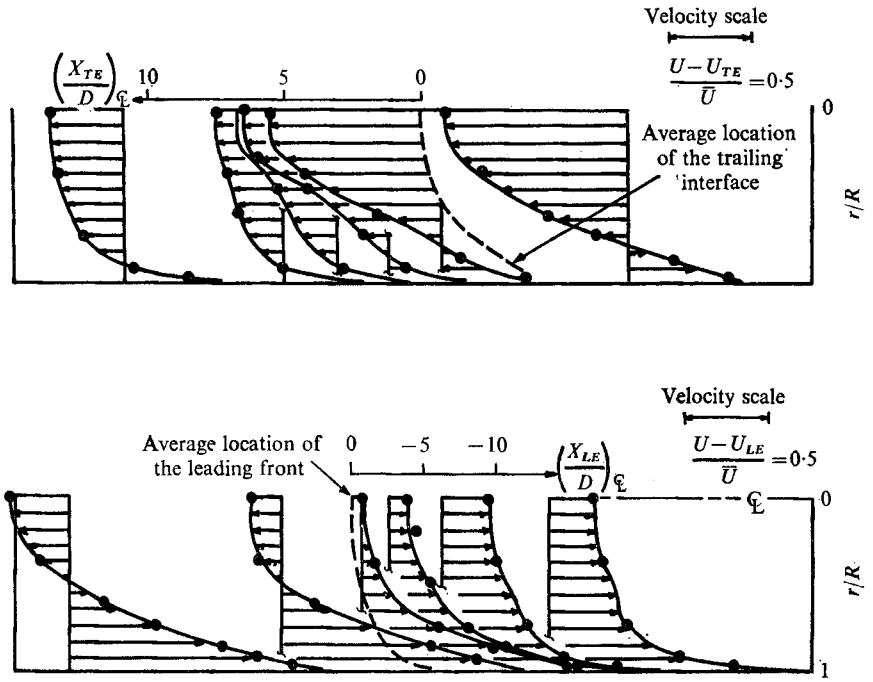

FIGURE 29. Velocity profiles relative to the leading and trailing fronts at $Re = 4200$ (the radial co-ordinate is stretched). $x/D = 505$, $U_{LE}/\bar{U} = 1{\cdot}45$, $U_{TE}/\bar{U} = 0{\cdot}746$.

a thicker sublayer. It seems plausible to conclude that *a unique relation exists between a velocity of a given interface and the velocity of the fluid, which prevents any turbulent fluid from leaving the slug.*

The computed streamlines relative to the respective interfaces at $Re = 19000$ are shown in figure 28, where the stream-function levels are defined by

$$\psi_{LE} = \int_0^r r(U-U_{LE})\,dr, \quad \psi_{TE} = \int_0^r r(U-U_{TE})\,dr.$$

Thus, provided that the mass flow remains constant, the difference between the stream functions at the wall is equal to

$$(\psi_{TE}-\psi_{LE})_{\text{wall}} = \tfrac{1}{2}(U_{LE}-U_{TE})\,R^2 \approx \tfrac{1}{2}\bar{U}R^2.$$

The leading interface is quite inactive in the central area of the pipe

$$(0 \leqslant r/R \leqslant \tfrac{1}{3}),$$

and in this respect it resembles the behaviour of a boundary-layer spot (Schubauer & Klebanoff 1955). The amount of fluid entrained by the leading interface per unit area increases monotonically with r/R. The trailing interface does not entrain any fluid near the wall and the amount of fluid entrained per unit area increases with decreasing radial distance from the centre-line.

The measurements described thus far were repeated at different Re with essentially the same results. The general conclusions relating the propagation of the turbulent interfaces and the mean motion are independent of Re although Re

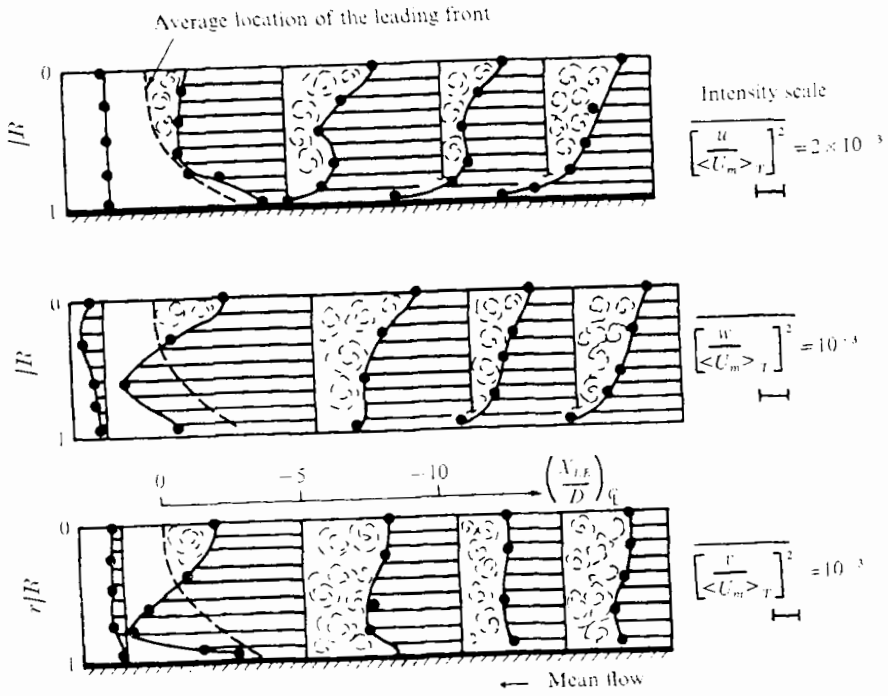

FIGURE 30. The three components of turbulent intensity near the leading interface. $Re = 1{\cdot}9 \times 10^4$, $x/D = 505$.

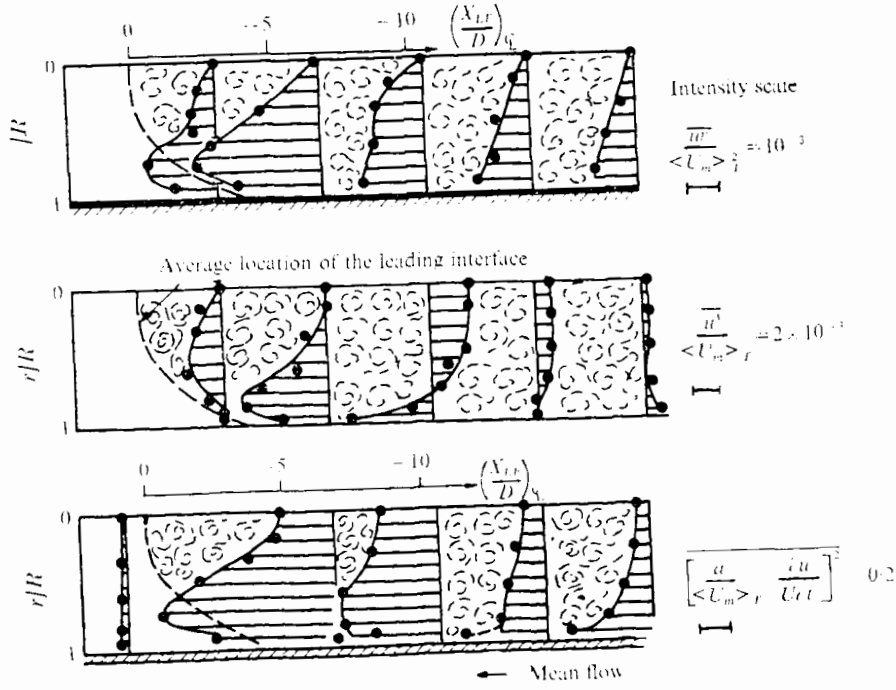

FIGURE 31. The distribution of shear stress $\overline{u^3}$ and $\overline{(\partial u/\partial t)^2}$ near the leading interface.

has an influence on the mean motion. In figure 29 a family of velocity profiles taken at $Re = 4200$ is shown. The radial co-ordinate is stretched relative to the distance from the interface in order to show in more detail the radial velocity distribution and the existence of the inflexion point.

The three components of the turbulent intensity, the shear stress, some third-order terms and temporal derivatives were also measured in the manner described earlier in this section. Some of the results are shown in figures 30 and 31. The relative length of the lines in each figure represents the magnitude of the quantity; the location of the base line corresponds to the appropriate distance of the measured profile from the interface. The results are rendered dimensionless by scaling them with the maximum velocity $\langle U_m \rangle_T$ at the centre-line deep in the interior of the slug.

The turbulent intensities imparted to the freshly entrained fluid exceed the level of fluctuations existing in the interior of the slug. It is this quality which enables a clear-cut distinction between the turbulent and laminar regions. It was reported by Klebanoff, Tidstrom & Sargent (1962), Elder (1960) and others (see Morkovin's (1969) review article) that very intense longitudinal fluctuations exist in boundary-layer flows just prior to breakdown to turbulence. Intensities in excess of 18 % of the free-stream velocity were encountered. Usually such a high turbulent intensity cannot be sustained in unseparated fully developed turbulent flows. The strong generation of turbulent energy may be associated with an inflexion in the mean velocity profile. Measurements by Klebanoff *et al.* (1962) on transition in a boundary layer indicated that the very rapid increase in intensity at breakdown to turbulence occurred simultaneously with an inflexion in the velocity profile. It now appears (Kline *et al.* 1967; Willmarth & Lu 1970) than even in fully developed turbulent boundary layers a momentary inflexion in the velocity distribution may be responsible for a strong production of turbulence. The turbulent levels encountered in the vicinity of the slug interface are generally speaking 4 to 7 times higher than in the interior of the slug. The maxima in the Reynolds stresses occur at approximately the same location as those at which an inflexion point is found.

We felt we could gain a better insight into the mechanism of slug propagation by comparing the various quantities at positions equidistant from the interface. We could have used the results already shown by replotting them, knowing the average shape of the interface, but we preferred to remeasure all the quantities in order to obtain better spatial resolution in the data. By positioning a turbulence detector upstream of the measuring station we have ensemble averaged the data assuming that at a constant Re all turbulent fronts propagate at the same velocity and have identical shapes. These assumptions are responsible for certain degradation in the spatial resolution. If one wishes to obtain measurements in co-ordinates which are moving with the interface and are parallel to it, one can use the same hot-wire output for the detection of turbulence as for the acquisition of the data. The ensemble averages obtained in this manner are independent of the speed and shape of the interface considered. The hot-wire signal which was used for data acquisition was delayed by a fixed period of time in order to provide us with data on the flow conditions which were prevalent

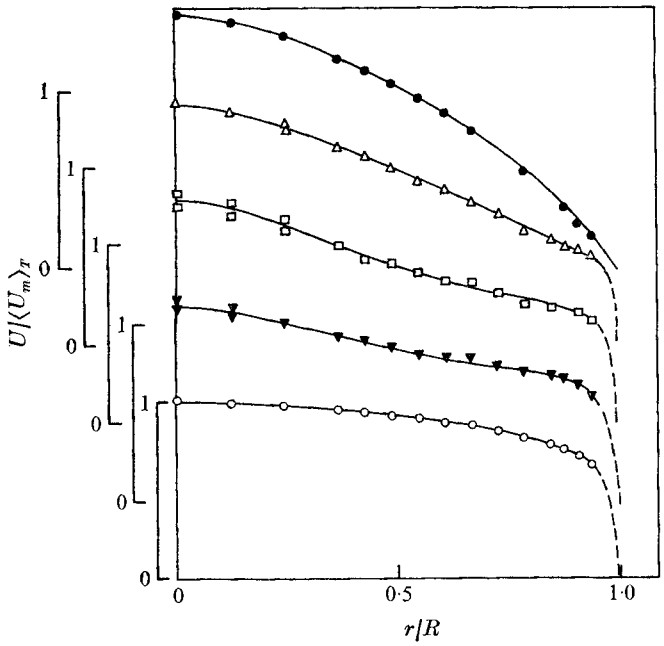

FIGURE 32. Ensemble-averaged velocity profiles in co-ordinates parallel to the leading front. $Re = 23700$, $x/D = 500$, $U_{LE}/\overline{U} = 1{\cdot}41$.

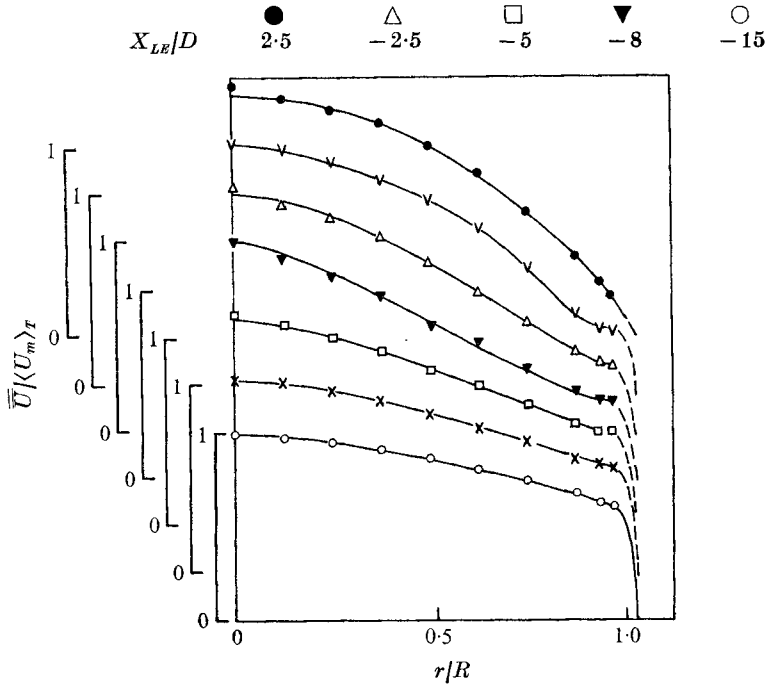

FIGURE 33. Ensemble-averaged velocity profiles in co-ordinates parallel to the trailing front. $Re = 23700$, $x/D = 500$, $U_{TE}/\overline{U} = 0{\cdot}32$.

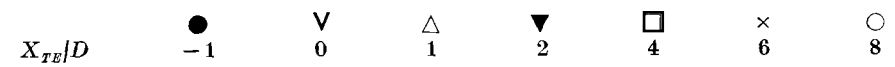

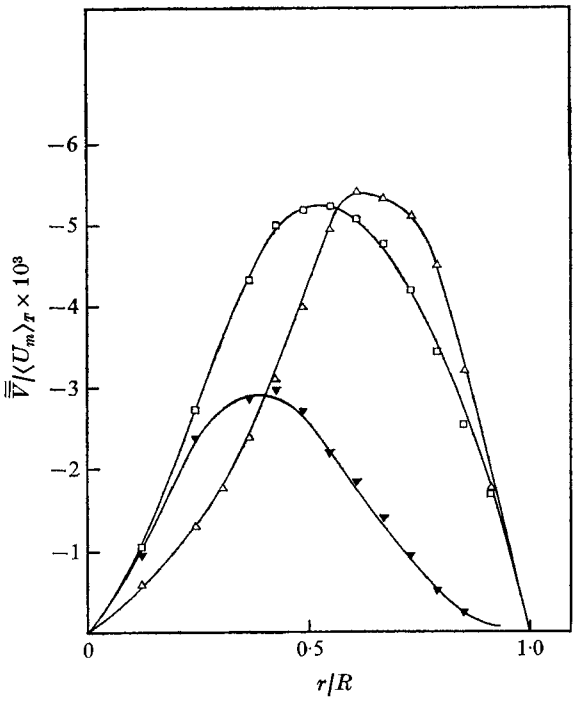

FIGURE 34. Calculated radial velocities at various distances from the leading front. $Re = 23700$, $x/D = 500$, $U/_{LE}\overline{U} = 1{\cdot}41$.

	△	□	▼
X_{LE}/D	−2·5	−5	−8

before the arrival of the interface. This is particularly important in the vicinity of the trailing edge.

The velocity profiles shown in figures 32 and 33 were obtained using the new technique. The double overbar in the figures indicates that the ensemble averaging was made parallel to the interface; all velocities were divided by the maximum velocity in the interior of the slug, so that 10 to 15 diameters away from the interface $\overline{\overline{U}}/\langle U_m\rangle_T = 1$. Near the leading interface $\overline{\overline{U}}$ still develops an inflexion point at $r/R \approx \frac{2}{3}$ and $-5 \leqslant X_{LE}/D \leqslant -10$, but the maximum values of $\partial U/\partial r$ are less than those observed in figure 23. The velocity distribution at $X_{LE}/D = 0$ is not shown because it is identical to that at $X_{LE}/D = 2{\cdot}5$, so the crossing of the interface has no immediate effect on the mean motion. On the other hand, the acceleration of the fluid near the wall at the trailing interface (figure 33) is very high. The inflexion point created as a result of this acceleration persists 4 diameters downstream of the interface but does not move inwards as in figure 24. The radial velocity $\overline{\overline{V}}$ near the leading interface (figure 34) is approximately the same as that shown in figure 25. However, at the average position of the trailing edge (figure 35) $\overline{\overline{V}}$ is higher than the radial velocity shown in figure 26.

In figures 36–38 the three components of the turbulent intensity are plotted against radius for various distances from the interface. A cross plot showing the continuous variation of $\overline{\overline{v^2}}$ with distance from the interface at given radii is

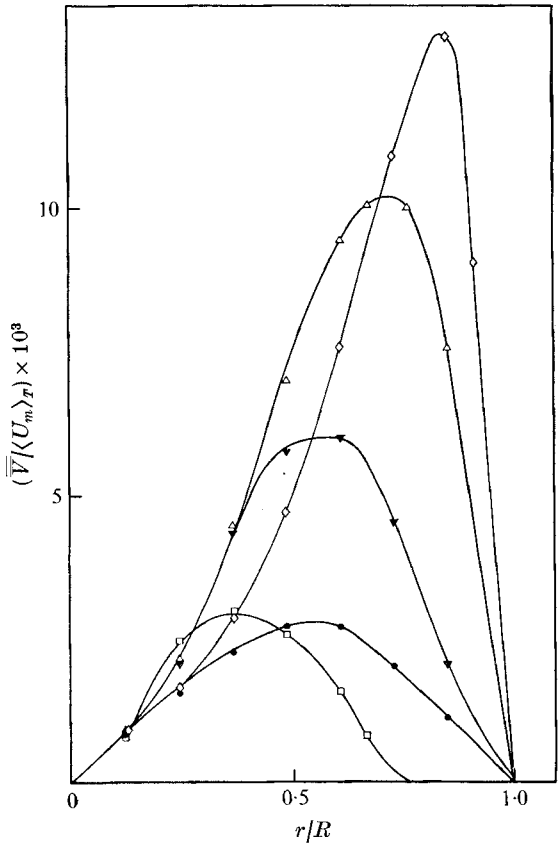

FIGURE 35. Calculated radial velocities at various distances from the trailing front. $Re = 23700$, $x/D = 500$, $U_{TE}/\bar{U} = 0{\cdot}32$.

X_{TE}/D	● −1	◇ 0	△ 1	▼ 2	□ 4

also shown in figure 37 (*b*) as an illustration of the manner in which data were obtained. Although the laminar flow preceding the slug is not free from disturbances, the almost catastrophic (two to three orders of magnitude) increase in the turbulent intensity over a length equivalent to a single pipe diameter is most impressive. A more careful examination of the figures reveals a certain correlation in the development of the turbulent flow. The longitudinal component $\overline{u^2}$ increases abruptly at the interface while the radial and transverse components $\overline{v^2}$ and $\overline{w^2}$ rise rather slowly. At $X_{LE}/D = 0$, u^2 increases to its highest value near the wall, and the location at which $\overline{u^2}$ has a peak moves towards the centre of the pipe with increasing distance into the slug. The value of the intensity at the peaks in the profiles remains fairly constant over the first five diameters away from the interface; it then deteriorates slowly while the intensity at the wall remains approximately constant for $X_{LE}/D \leqslant -5$. The radial fluctuations $\overline{v^2}$ reach their maximum at $X_{LE}/D = -2{\cdot}5$. The peak does not occur near the wall but at $r/R = 0{\cdot}8$, and it decays as the distance from the interface increases. The

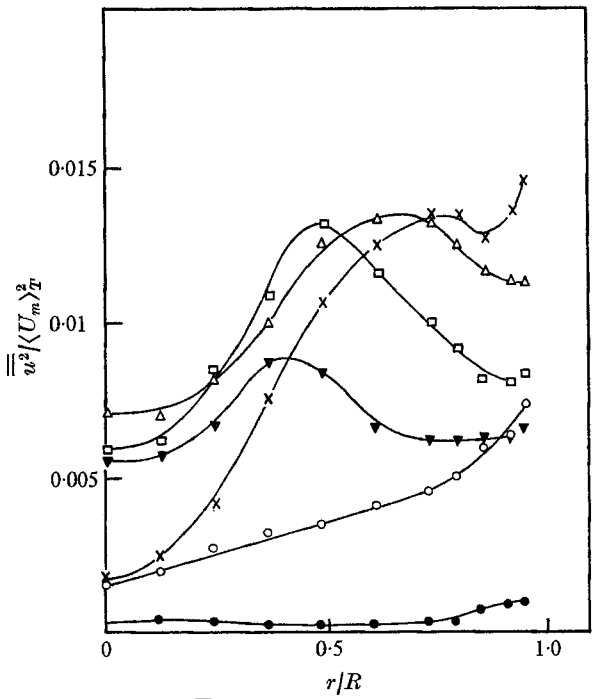

FIGURE 36. The distribution of $\overline{\overline{u^2}}$ at various distances from the leading front. $Re = 23700$, $x/D = 500$, $U_{LE}/\bar{U} = 1{\cdot}41$.

	●	×	△	□	▼	○
X_{LE}/D	2·5	0	−2·5	−5	−8	−15

transverse fluctuations $\overline{\overline{w^2}}$ attain their maximum level even further downstream from the leading front, i.e. at $X_{LE}/D \approx -5$ and $r/R \approx \frac{2}{3}$. The sequence in which the three components of the turbulent fluctuations reach their maxima fits very well Theodorsen's (1955) horseshoe vortex model of the turbulent boundary layer and the explanation of Kline *et al.* (1967) of the streaky structure of the flow near a solid surface. The evidence suggests the mechanism which is sketched in figure 39 (plate 5). The streamline pattern in a frame moving with the leading front (figure 28) is only quasi-steady. It shows the existence of a very large elongated ring vortex near the centre of the pipe. One may envisage a series of such eddies as shown in figure 39(*a*). The physical picture is consistent with the oscillatory behaviour of a hot-wire trace in the laminar region and it is similar to a series of eddies observed near a forward-facing step. The radial velocity (downwash) existing between the first two eddies may convect the second eddy or the rear portion of the first eddy away from the centre into a region of very strong mean shear and relatively high velocity (figure 39*b*). The rapid stretching can rupture the ring vortex and the downward motion will further stretch the remnants until a critical scale is reached (the scale refers to both a diameter of a particular vortex tube and to the distance between adjacent tubes) near the interface causing a sudden and complete disintegration as shown in figure 37.

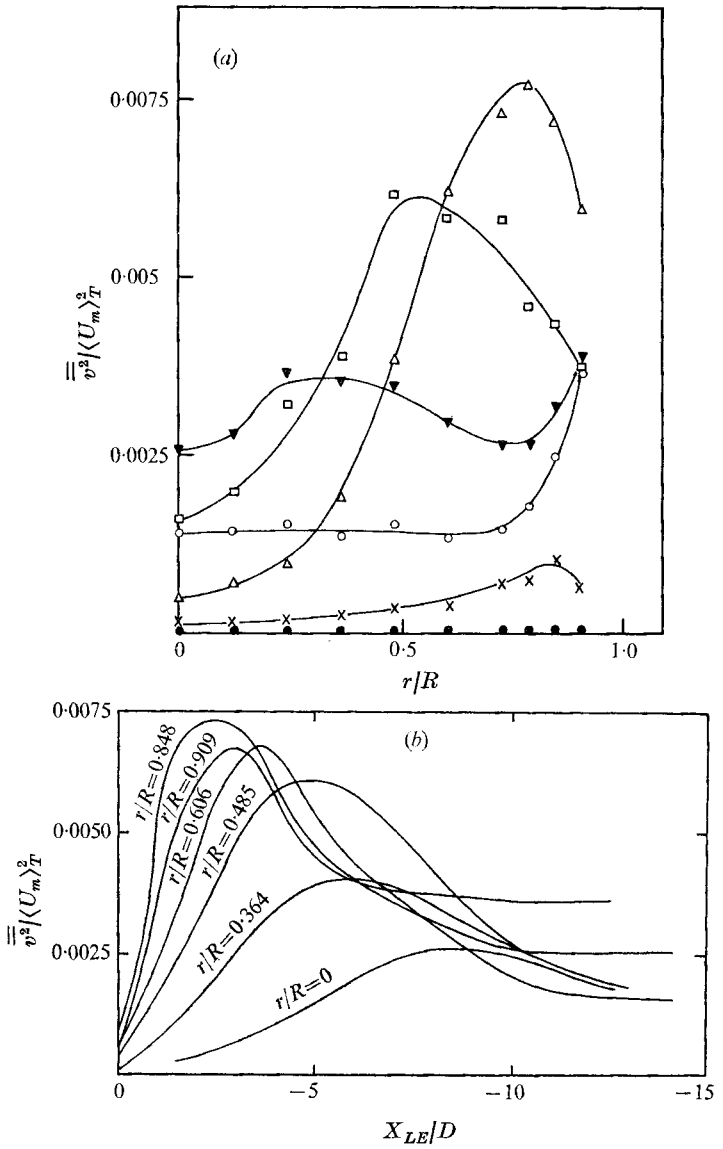

FIGURE 37. (*a*) The distribution of $\overline{v^2}$ at various distances from the leading front. (*b*) The variation of $\overline{v^2}$ with distance from the leading front at constant radial location. Re = 23700, x/D = 500, $U_{TE}/\bar{U}$ = 1·41. Symbols as in figure 36.

The longitudinal vortices created by the initial stretching will probably disintegrate faster as they come in pairs of opposing vorticity. A sudden burst of a vortex is a familiar phenomenon in aeronautics: leading-edge vortices on slender bodies and delta wings are known for their sudden disintegration (Lowson 1964). The explanation of bursting may differ from case to case but the abruptness of the phenomenon is not disputed. The end result of the disintegration is a series of eddies in the wall region of the leading interface which are small when compared with the semi-stationary eddy in the central core of the pipe on the laminar

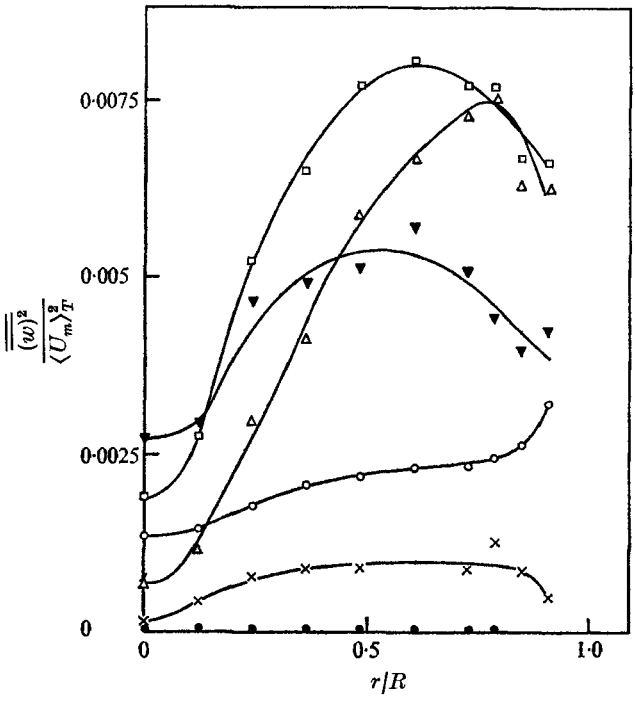

FIGURE 38. The distribution of $\overline{\overline{w^2}}$ at various distances from the leading front. Re = 23700, x/D = 500, $U_{LE}/\bar{U}$ = 1·41. Symbols as in figure 36.

side of the interface, but are large when compared with various turbulent scales. The radial fluctuations associated with a flattened 'spanwise' eddy near the wall of the pipe must be smaller than the longitudinal fluctuations which are not inhibited as much by the solid surface (i.e. $\overline{\overline{u^2}} > \overline{\overline{v^2}}$). The tangential fluctuations are primarily associated with the meandering of the vortex lines and are also small in comparison with $\overline{\overline{u^2}}$. Since the fluid near the wall undergoes a deceleration as it proceeds into the slug, the eddy will be compressed and may eventually buckle towards the centre of the pipe (figure 39*d*). The repeatable buckling or thickening of the vortex may be associated with the observed inflexion in the ensemble-averaged velocity distribution. One would also observe an increase in $\overline{\overline{v^2}}$ resulting from the increased distance between the eddy and the wall and an increase in $\overline{\overline{w^2}}$ resulting from distorting the eddy. Mean shear will act again to stretch and distort the eddy further, producing a typical horseshoe vortex. At this stage one would expect $\overline{\overline{w^2}}$ to increase somewhat as a result of the distortion. If a longitudinal eddy were to exist near the wall at the interface it would be similarly affected by the deceleration of the mean flow and would eventually change into a horseshoe vortex. The maxima of all three components of the fluctuations should follow the core of the eddy and move towards the centre of the pipe, as they indeed do. At a distance from the interface corresponding to the region where a horseshoe vortex prevails one may expect two maxima in $\overline{\overline{u^2}}$, $\overline{\overline{v^2}}$ and $\overline{\overline{uv}}$ to develop, one at the base of the horseshoe vortex near

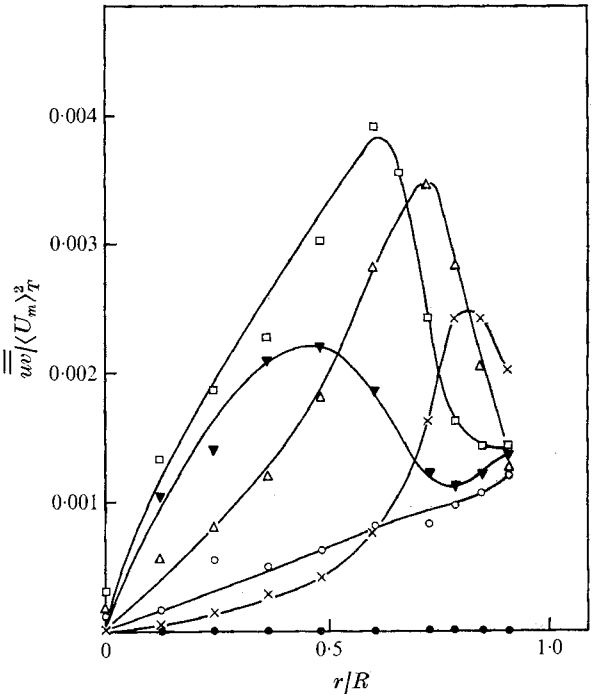

FIGURE 40. The distribution of shear stress at various distances from the leading front. $Re = 23700$, $x/D = 500$, $U_{LE}/\overline{U} = 1{\cdot}41$. Symbols as in figure 36.

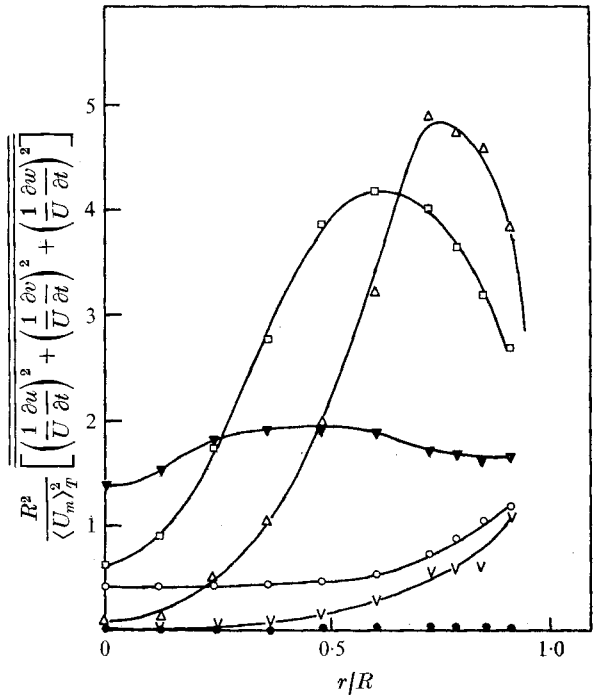

FIGURE 41. The distribution of dissipation terms at various distances from the leading front. $Re = 23700$, $x/D = 500$, $U_{LE}/\overline{U} = 1{\cdot}41$.

	●	∨	△	□	▼	○
X_{LE}/D	2·5	0	−2·5	−5	−8	−15

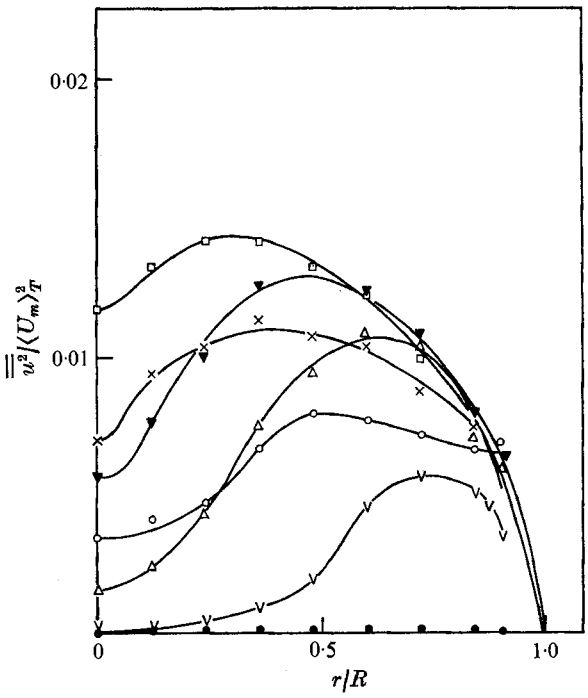

FIGURE 42. The distribution of $\overline{u^2}$ at various distances from the trailing front. Re = 23700, x/D = 500, $U_{TE}/\overline{U}$ = 0·32.

X_{TE}/D	● −1	V 0	△ 1	▼ 2	□ 4	× 6	○ 8

the wall and a stronger one at the toe of the horseshoe vortex away from the wall. One may indeed notice this trend in figures 36, 37 and 40 at $X_{LE}/D = 8$. The measured shear stress should slowly increase as the vortex undergoes stretching and as long as it remains coherent. The shear stress increases for the first 5 diameters away from the interface and the radial location of the peak moves towards the centre in the process. A process similar to the one shown in figure 39 (*d*) probably repeats itself on a smaller scale in the interior of the slug as it does in the fully developed boundary layer, and may be considered as the physical mechanism contributing to turbulence production. Even near the interface small-scale eddies are present. According to Theodorsen (1955) one may find those eddies wrapped around the large-scale horseshoe vortex.

The sum of the measured terms responsible for dissipation is plotted in figure 41. Because the large eddies are almost independent of viscosity, the terms contributing to dissipation initially increase quite slowly. As we shall see later, the dissipation terms do not balance production for the first 15 diameters away from the interface. The radial distribution of the derivatives measured follows approximately the same pattern as the intensities do.

The radial distributions of the three components of the turbulent intensity near the trailing interface are plotted in figures 42–44, and another cross plot showing a continuous variation of $\overline{v^2}$ with distance from the trailing interface is

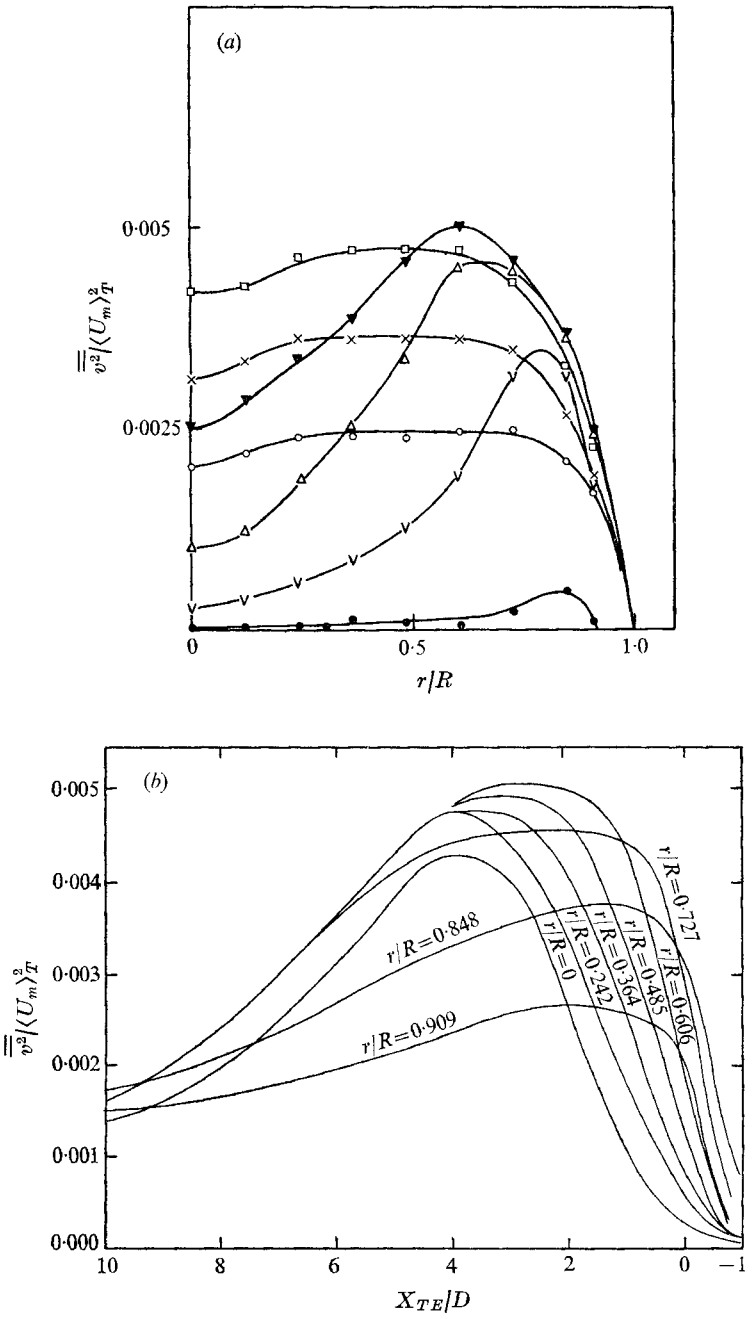

FIGURE 43. (*a*) The distribution of $\overline{\overline{v^2}}$ at various distances from the trailing front. (*b*) The variation of $\overline{\overline{v^2}}$ with distance from the trailing front at constant radial location. Re = 23 700, x/D = 500, $U_{TE}/\bar{U}$ = 0·32. Symbols as in figure 42.

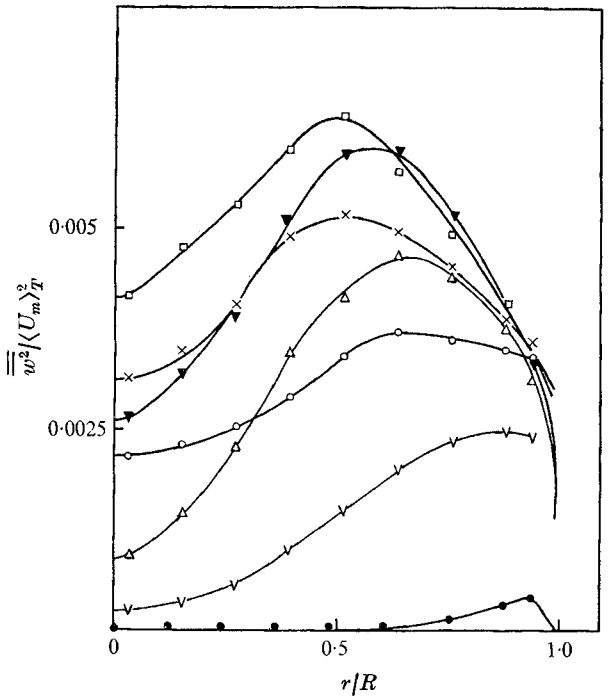

FIGURE 44. The distribution of $\overline{\overline{w^2}}$ at various distances from the trailing front. $Re = 23\,700$, $x/D = 500$, $U_{TE}/\overline{U} = 0{\cdot}32$. Symbols as in figure 42.

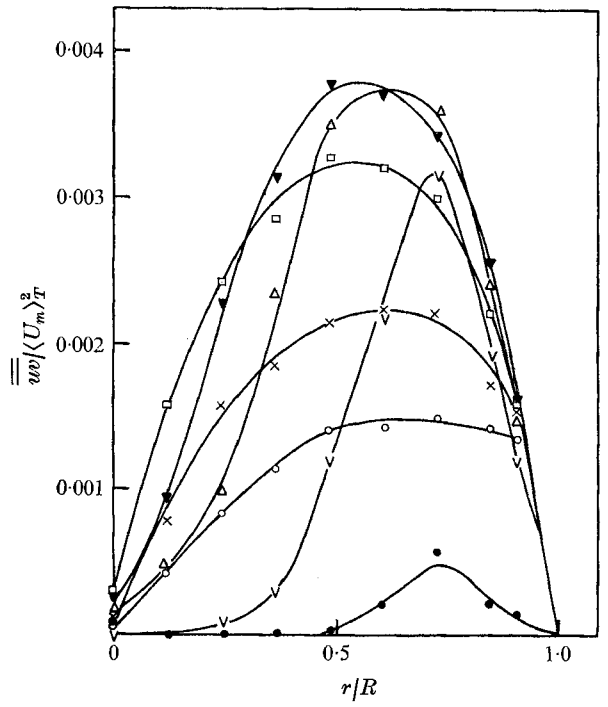

FIGURE 45. The distribution of $\overline{\overline{uv}}$ at various distances from the trailing front. $Re = 23\,700$, $x/D = 500$, $U_{TE}/\overline{U} = 0{\cdot}32$. Symbols as in figure 42.

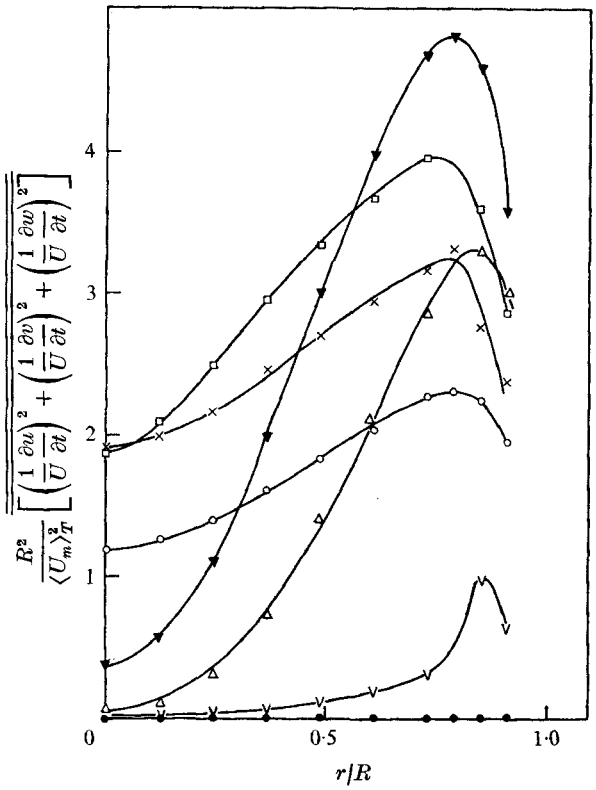

FIGURE 47. The distribution of dissipation terms at various distances from the trailing front. Symbols as in figure 42.

given in figure 43(*b*). The shear stress is plotted in figure 45. The intensity of turbulence increases initially with increasing X_{TE} and attains its maximum level at $X_{TE}/D = 4$. The radial distribution of each component near the leading front differs from the radial distribution of the same component near the trailing front because the maxima in the latter case no longer occur as close to the wall. Although the ensemble-averaged velocity distribution exhibits a strong inflexion point at $r/R \approx 0{\cdot}9$ (figure 33), there is a relative weakness in the turbulent activity near the solid surfaces. This is attributed to the acceleration of the flow near the surface at the trailing edge, in contrast to the deceleration which occurs near the leading front. The large ring vortex existing near the wall at the trailing edge (figure 28) may intermittently disintegrate and contribute heavily to the turbulent eddies found near the interface. However, as a result of the accelerating mean flow near the wall, a 'spanwise' eddy would find itself initially in a stable environment. Nevertheless, a rapid stretching mechanism is possible as a result of the secondary flow which is associated with the inflow towards the wall. The secondary flow will produce large longitudinal vortices and will render the spanwise eddies unstable by pulling them away from the wall (figure 46, plate 6). This mechanism must be quite efficient because the maximum values of the turbulent intensities near the trailing edge are comparable with those at the

leading edge in spite of the initial stabilizing effect resulting from the accelerating mean motion. While most of the turbulent intensities peak near $r/R \approx 0{\cdot}5$, the dissipation terms are a maximum much closer to the wall (figure 47). The dissipation terms are again small when compared with production terms in the energy budget. Before passing on to another subject, we should like to stress the fact that the vortex model is highly oversimplified and conjectural. However, it easily explains the general trend of the observations.

We shall now examine the budget of turbulent energy near leading and trailing interfaces of a typical slug. The customary manipulation of the momentum, continuity and kinetic energy equations for a frame moving with the interface yields

$$(U-U_F)\frac{\partial q}{\partial x}+V\frac{\partial q}{\partial r}+2\left[(\overline{u^2}-\overline{v^2})\frac{\partial U}{\partial x}+(\overline{w^2}-\overline{v^2})\frac{V}{r}+\overline{uv}\left(\frac{\partial U}{\partial r}+\frac{\partial V}{\partial x}\right)\right]$$

Convection Production

$$+\frac{\partial}{\partial x}(\overline{uq})+\frac{1}{r}\frac{\partial}{\partial r}(r\overline{vq})+\frac{2}{\rho}\left[\frac{\partial}{\partial x}(\overline{up})+\frac{1}{r}\frac{\partial}{\partial r}(r\overline{vp})\right]$$

Diffusion

$$-\nu\left[\nabla^2(q)-2\left(\frac{\overline{v^2}+\overline{w^2}}{r^2}\right)-2\overline{\left(\frac{\partial u_i}{\partial x_j}\right)^2}\right]=0,$$

Dissipation

where $q=\overline{u^2}+\overline{v^2}+\overline{w^2}$, U_F is the velocity of the front, $U_F=U_{LE}$ near the leading interface and $U_F=U_{TE}$ near the trailing interface. In deriving this equation, we assumed that the flow is symmetric about the centre-line of the pipe and that there is no swirl. Thus, all the derivatives with respect to the azimuthal angle ϕ were neglected. Furthermore, $\partial V/\partial x$ and $\nu[\nabla^2(q)-2(\overline{v^2}+\overline{w^2})/r^2]$ may also be neglected because $\partial U/\partial r \gg \partial V/\partial x$ (the ratio is about 10^4) and similarly

$$\overline{\left(\frac{\partial u_i}{\partial x_j}\right)^2} \gg \nabla^2 q-2\frac{\overline{v^2}+\overline{w^2}}{r^2}.$$

All the significant terms contributing to convection and production of turbulent energy are known. The dissipation term can be constructed upon the assumption of partial small-scale isotropy

$$\overline{(\partial u_i/\partial x_j)^2}=3\overline{(\partial u_i/\partial x)^2},$$

and the total diffusion term is obtained from the equation. The energy balances were performed for a co-ordinate system parallel to the interface, as used in figure 32 and thereafter.

Figure 48 shows the radial distribution of energy balance at five distances from the leading front. For ease of comparison the energy budget has been replotted as a function of the distance from the interface for three radial locations in figure 49. The largest single term near the leading front is the production of

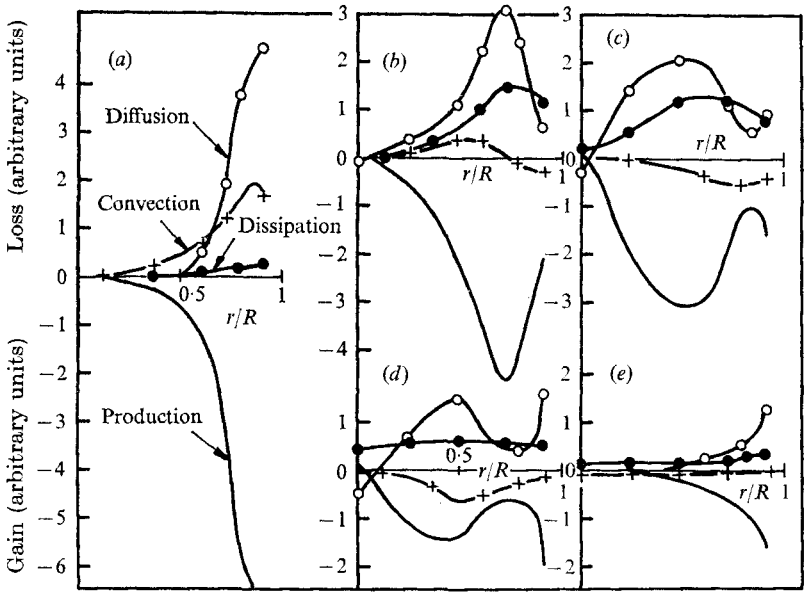

FIGURE 48. The turbulent energy balance at constant distances from the leading front. (*a*) $X_{LE}/D = 0$; (*b*) $X_{LE}/D = -2{\cdot}5$; (*c*) $X_{LE}/D = -5$; (*d*) $X_{LE}/D = -8$; (*e*) $X_{LE}/D = -15$.

turbulent energy. The production term is strongest at the interface and very near to the wall. Although $\overline{uv}$ increases with increasing distance from the interface (for $X_{LE} \geqslant -5$) the maximum in the production term drops continuously with this distance. This is so because the eddying motion affects the mean velocity distribution by reducing $\partial U/\partial r$. Since the maximum of the production term moves towards the axis of the pipe with increasing distance from the interface, the production term integrated over a given cross-sectional area reduces even faster with increasing X_{LE} than a comparison of the peaks in figure 48 would indicate. Some characteristic values are given in table 1. The integrated dissipation term at the interface is very small but it increases with decreasing X_{LE} until $X_{LE}/D \approx -5$. It then drops to a value which is approximately equal to the integrated production at $X_{LE}/D < -20$. Since only the smallest eddies contribute to dissipation, a certain time is required for the cascading process to take effect. At the interface the integrated production is 23 times larger than the integrated dissipation. At $X_{LE}/D = -5$ the ratio between production and dissipation drops to a local minimum level of 2. The cross-section at which the minimum occurs coincides with the cross-section at which the turbulent intensities attain their maxima. For $-15 \leqslant X_{LE}/D \leqslant -5$, the ratio between the integrated production and dissipation increases slightly while the turbulent intensities are decreasing; it eventually drops to its equilibrium level in the interior of the slug. The relationship between production, dissipation and local turbulent intensity is in general agreement with the basic entrainment hypothesis of Townsend (1966). He suggested that the mechanism of entrainment by free turbulent shear flows is largely controlled by the intensity of the large eddies which contort the interface and increase the surface area across which diffusion of small-scale vorticity can take

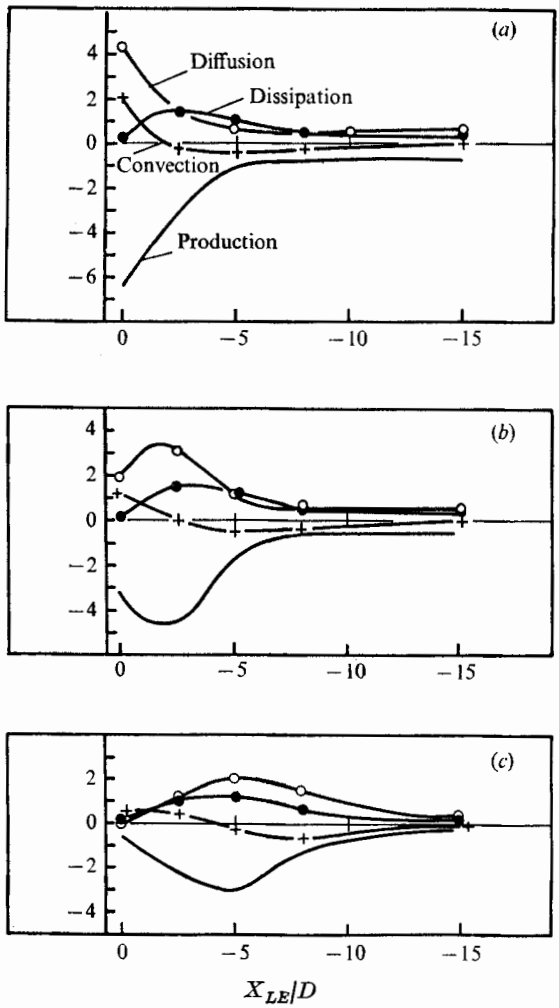

FIGURE 49. A cross plot of the turbulent energy balance at constant radial locations near the leading interface. (*a*) $r/R = 0{\cdot}85$; (*b*) $r/R = 0{\cdot}728$; (*c*) $r/R = 0{\cdot}5$.

X_{LE}/D	0	−2·5	−5	−8	−15
$\dfrac{\text{Integrated production}}{(\text{Integrated production})_{LE}}$	1	0·785	0·605	0·374	0·237
$\dfrac{\text{Integrated dissipation}}{(\text{Integrated production})_{LE}}$	0·043	0·296	0·302	0·167	0·071

TABLE 1

place. Those eddies derive their energy from the mean motion, while the remaining smaller scale turbulent eddies restrain the growth of the large eddies by absorbing part of their energy. The equilibrium hypothesis states that the large eddies build their own mechanism of destruction by causing a large increase in the rate of production of turbulent energy. Townsend envisages the following

operational cycle: "growth of large eddies → rapid entrainment and production → increase of turbulent intensity → damping of large eddies → decrease of intensity...". This mechanism was suggested for the entrainment of irrotational fluid in free turbulent shear flows. In transitional pipe flow the interface is normal to the mean motion and the fluid is rotational on both sides of the interface. Corrsin & Kistler (1955) point out that the dominant turbulence propagation mechanism may be different in this case. "In particular, it may be that a destabilization of the already rotational flow occurs in addition to a transmission of random vorticity by direct viscous action at the turbulent–laminar interface." One may, however, examine the present data in the light of Townsend's hypothesis and observe at least one definitive operational cycle by considering the turbulent flow moving away from the interface. The strong entrainment of non-turbulent fluid at the leading front near the wall is accompanied by a strong production. The turbulent intensities increase, reducing the ratio between production and dissipation. As the large eddies are quenched, their contribution to production reduces, bringing about a reduction in intensity and thus permitting reorganization of the large motion and regeneration of the process.

The turbulent intensities attain their maxima near the wall at $X_{LE}/D \approx -2$ as a result of the strong production in that region. At the centre of the pipe the turbulent intensity peaks at $X_{LE}/D \approx -5$, because the convection along the axis of the pipe is much larger than convection in the radial direction. Turbulence near the wall loses energy by convective action as long as $X_{LE}/D \geqslant -2$; thereafter convection changes sign in the vicinity of the wall. At a distance larger than 5 diameters from the interface the convective process contributes to the gain of turbulent energy across the entire pipe cross-section.

The total diffusion process, including pressure–velocity correlations, makes the largest contribution to the loss of turbulent energy for the first 15 diameters away from the interface. For $X_{LE}/D < -6$, the dissipation term approximately balances the convection term, leaving production and diffusion to balance one another.

The energy balance at $X_{LE}/D = 0$ shows that entrainment of non-turbulent fluid is closely tied to the magnitude of the various terms in the energy budget. If all the terms contributing to the turbulent energy budget vanish identically anywhere on the interface then that portion of the interface does not entrain any non-turbulent fluid. A comparison between the left-hand part of figure 48 and the entrained streamline pattern in figure 28 confirms this point. It appears from energy considerations that gradient diffusion (including the pressure transport term) is most likely the term responsible for the propagation of the leading interface. Because the mean flow convects the turbulent energy towards the interior of the slug, the remaining excess of energy produced is transported towards the interface by diffusion. The gradient of intensity in the direction normal to the interface is very strong near the leading edge, particularly in the vicinity of the wall. It thus can be the only mechanism pushing the locally produced turbulent energy in the direction of the flow. Since $(\partial q/\partial r)_{LE} \leqslant 0$ the turbulent energy also diffuses radially from the wall towards the centre of the pipe. Figure 49 shows that entrainment may be correlated with the existence of

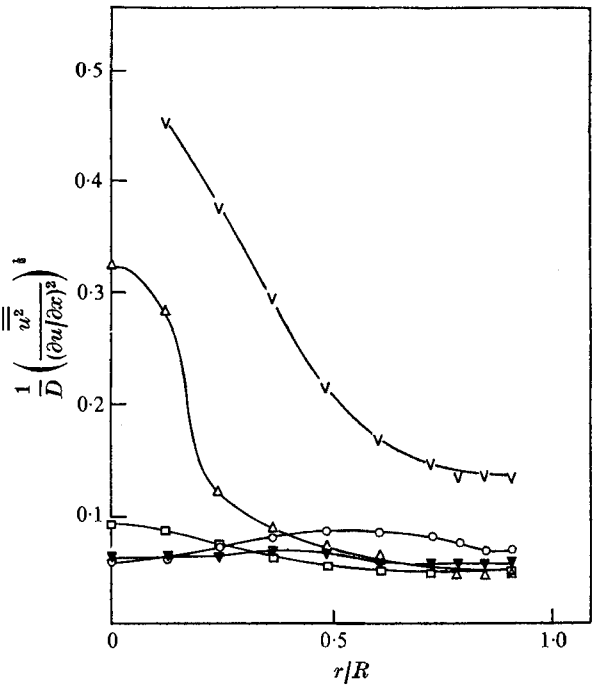

FIGURE 50. The Taylor microscales near the leading interface. Re = 23700, x/D = 500, $U_{LE}/\overline{U}$ = 1·41.

	∨	△	▼	□	○
X_{LE}/D	0	−2·5	−5	−8	−15

peaks in both the production and diffusion terms at the interface and the magnitudes of the peaks.

In figure 50 the dimensionless Taylor microscales near the leading edge of a slug are plotted. Although λ_f is considerably larger than the scale of the dissipation eddies and smaller than the scale of the energy-containing eddies (Townsend 1956), it is none the less a useful parameter for representing a ratio between the turbulent intensity and the dissipation. One may notice that this ratio is very large at the interface, but it drops very quickly to its equilibrium level. Indeed at $X_{LE}/D = -5$, an equilibrium between the intensity and the dissipation has almost been attained across the entire cross-section of the flow.

The energy balance near the trailing front is plotted in figures 51 and 52 and enables us to compare the behaviour of the flow near both interfaces. The production of turbulent energy near the trailing front is again the single largest term in the energy budget. However, while the peak in production near the leading edge occurs at the wall the largest production near the trailing interface occurs approximately at $r/R = \frac{3}{4}$. In both cases the maxima of production and diffusion at the interface correspond to the location at which the entrainment of non-turbulent fluid is highest. Since the trailing interface does not entrain any fluid near the wall, all the terms in the energy budget near the wall become negligible. It again appears that diffusion is the only recognizable mechanism by which

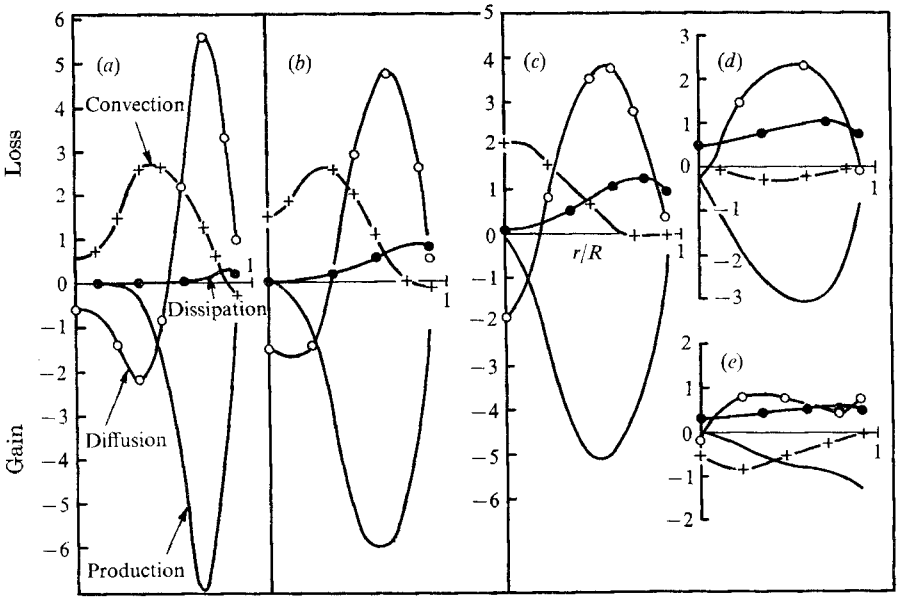

FIGURE 51. The turbulent energy balance at constant distances from the trailing front. (*a*) $X_{TE}/D = 0$; (*b*) $X_{TE}/D = 1$; (*c*) $X_{TE}/D = 2$; (*d*) $X_{TE}/D = 4$; (*e*) $X_{TE}/D = 8$.

X_{TE}/D	0	1	2	4	6	8
$\dfrac{\text{Integrated production}}{(\text{Integrated production})_{TE}}$	1·00	1·25	1·10	0·732	0·448	0·302
$\dfrac{\text{Integrated dissipation}}{(\text{Integrated production})_{TE}}$	0·0319	0·197	0·317	0·296	0·245	0·177

TABLE 2

turbulent energy can be transferred into the non-turbulent fluid. The radial gradient of intensity $[(\partial q/\partial r)_{TE} < 0$ for $0 \leqslant r/R \leqslant 0{\cdot}8]$ enables the turbulent energy to diffuse towards the centre of the pipe and counteract the loss of energy resulting from convection. The loss of turbulent energy by convection in the central region of the pipe for $0 \leqslant X_{TE}/D \leqslant 3$ presents an immediately apparent difference between the leading and trailing fronts.

The maximum in the production term drops with increasing distance into the slug from the trailing interface, just as the maximum of the production dropped upstream of the leading interface. The production integrated over the cross-section of the pipe, however, does not fall off monotonically with increasing distance from the interface as it did near the leading front. Some characteristic numbers are given in table 2. The fact that the production is not highest right at the trailing interface may be associated with the initial stability near the wall as a result of the local acceleration there. At the interface the integrated production is 31 times larger than the integrated dissipation. At $X_{TE}/D = 4$ (the distance from the interface at which the turbulent intensities attain approxi-

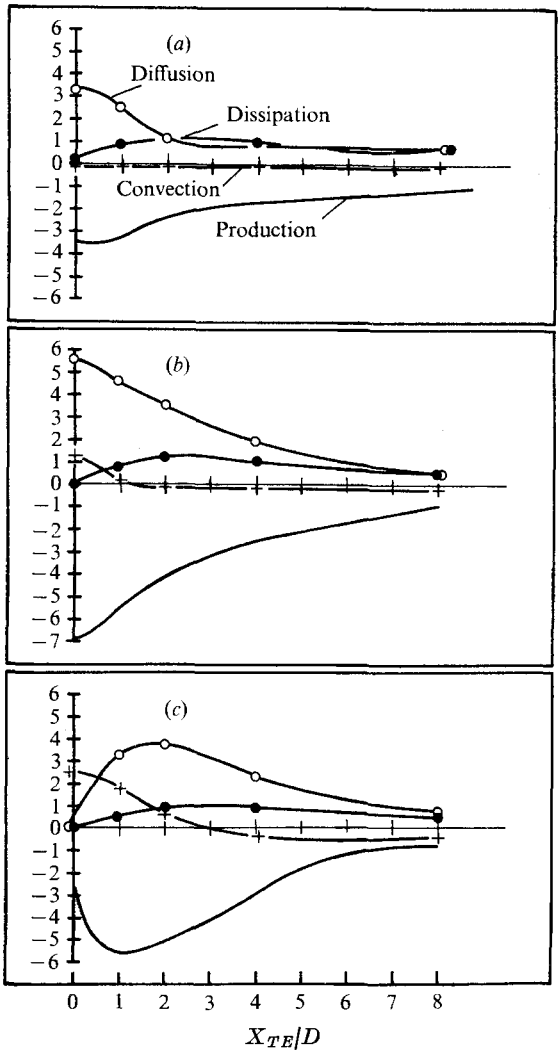

FIGURE 52. A cross plot of the turbulent energy balance at constant radial locations near the trailing interface. (*a*) $r/R = 0{\cdot}85$; (*b*) $r/R = 0{\cdot}728$; (*c*) $r/R = 0{\cdot}5$.

mately their maxima), the ratio between the integrated production and dissipation decreases to 2·5. These ratios are similar to the ratios observed near the leading front.

Since the trailing front moves downstream at $U_{TE} \approx \frac{1}{3}\overline{U}$, the velocities relative to the trailing interface are much smaller than the velocities relative to the leading interface, which moves at a speed $U_{LE} \approx \frac{3}{2}\overline{U}$. Consequently various characteristic time scales are larger and the flow can adjust to its new fully developed turbulent character at a shorter distance from the trailing interface than from the leading one. The relatively long residence time may enable the smaller scale turbulent eddies to destroy any coherency in the large eddying motion. The equilibrium cycle suggested by Townsend may thus not be visible near the trailing interface. The ratio between the production and dissipation

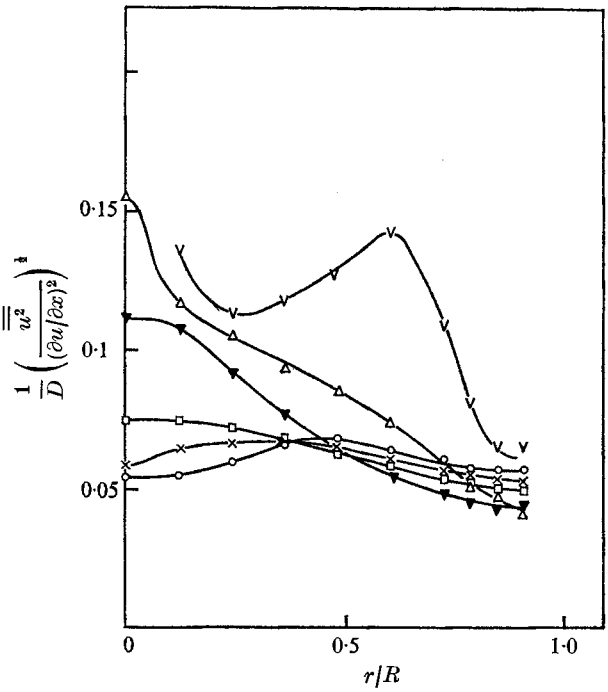

FIGURE 53. The Taylor microscales near the trailing interface. $Re = 23700$, $x/D = 500$, $U_{TE}/\bar{U} = 0{\cdot}32$.

	▽	△	▼	□	×	○
X_{TE}/D	0	1	2	4	6	8

integrated across the pipe drops monotonically with increasing distance from the trailing front and does not increase again as the turbulent intensities decrease at $X_{TE}/D > 4$. It should be recalled that such an increase was noticeable near the leading front.

Because $\partial q/\partial x < 0$ at $X_{TE}/D \geqslant 4$, the convection term changes its sign near $X_{TE}/D = 4$. Eight diameters away from the trailing interface, the production and dissipation attain a radial distribution similar to that in the interior of the slug, although an intensity gradient in the axial direction still exists. In figure 52 one may notice the relative slowness with which the dissipation builds up with increasing distance from the interface. It appears therefore that the cascading process leading to the production of small dissipative eddies responds relatively slowly to changes in the large-scale motion. Near the trailing front the Taylor microscales (figure 53) are greater than in the interior of the slug, but not as large as the microscales near the leading front at the same location relative to the interface.

The emphasis in this paper was placed on describing the flow in a turbulent slug. The structure of the puff will be presented together with the results obtained in a controlled transition experiment which is currently underway.

The authors wish to express their gratitude to F. Lange for his continuous assistance, to T. Deaton for designing the time delay circuit, and to A. Green-

berger for his beautiful machining work. We also wish to thank S. C. Crow for reading and commenting on the manuscript.

The project was initiated at the Israel Institute of Technology, where the first author spent a Sabbatical year. During the final and most fruitful year of its duration, the project was sponsored by the Air Force Office of Scientific Research (AFSC), United States Air Force, under contract F44620-71-C-0079.

REFERENCES

CHRISTIANSEN, E. B. & LEMMON, H. E. 1965 *A.I.Ch.E. J.* **11**, 995.

COLES, D. 1962 In *Mécanique de la Turbulence* (ed. A. Favre), pp. 229. Paris: C.N.R.S.

CORRSIN, S. & KISTLER, A. 1955 *N.A.C.A. Rep.* no. 1244.

CROW, S. C. & CHAMPAGNE, F. H. 1971 *J. Fluid Mech.* **48**, 547.

ELDER, J. W. 1960 *J. Fluid Mech.* **9**, 235.

GOLDSTEIN, S. (ed.) 1938 *Modern Developments in Fluid Dynamics.* Oxford University Press.

KIBENS, V. 1968 Ph.D. dissertation, Department of Mechanics, Johns Hopkins University.

KLEBANOFF, P. S., TIDSTROM, K. D. & SARGENT, L. M. 1962 *J. Fluid Mech.* **12**, 1.

KLINE, S. J., REYNOLDS, W. C., SCHRAUB, F. A. & RUNSTADLER, P. W. 1967 *J. Fluid Mech.* **30**, 741.

KOVASZNAY, L. S. G., KOMODA, H. & VESUDEVA, B. R. 1962 *Proc. Heat Trans. & Fluid Mech. Inst.* Stanford University Press.

LAUFER, J. 1954 *N.A.C.A. Rep.* no. 1174.

LINDGREN, E. R. 1957 *Arkiv Fys.* **12**, 1.

LINDGREN, E. R. 1969 *Phys. Fluids*, **12**, 418.

LOWSON, M. V. 1964 *J. Roy. Aero. Soc.* **68**, 343.

MICHALKE, A. & WILLE, R. 1964 *Proc. of the* 11*th Int. Cong. Appl. Mech.* (ed. H. Görtler). Springer.

MORKOVIN, M. V. 1969 *Viscous Drag Reduction.* Plenum Press.

PATEL, R. R. 1968 *McGill Univ. Dept. Mech. Engng Rep.* no. 68–7.

PATEL, V. C. & HEAD, M. R. 1969 *J. Fluid Mech.* **38**, 181.

RESHOTKO, E. 1958 *Jet Propulsion Lab., Pasadena, Prog. Rep.* no. 20–364.

REYNOLDS, O. 1883 *Phil. Trans.* **174**, 935.

ROTTA, J. 1956 *Ing. Arch.* **24**, 258.

SCHUBAUER, G. B. & KLEBANOFF, P. S. 1956 *N.A.C.A. Rep.* no. 1289.

SMITH, A. M. O. 1960 *J. Fluid Mech.* **7**, 565.

TATSUMI, T. 1952 *J. Phys. Soc. Japan*, **7**, 489.

THEODORSEN, T. 1955 In *Fifty Years of Boundary Layer Research* (ed. H. Görtler), pp. 55–63. Braunschweig: Friedr. Vieweg.

TOWNSEND, A. A. 1956 *The Structure of Turbulent Shear Flow.* Cambridge University Press.

TOWNSEND, A. A. 1966 *J. Fluid Mech.* **26**, 689.

VALERANI, E. 1964 Engineer's thesis, Guggenheim Aero. Lab., Calif. Inst. Tech.

WILLMARTH, W. W. & LU, S. S. 1970 *Bull. Am. Phys. Soc. Ser.* II, **15**, 1545.

WYGNANSKI, I. 1971 *Israel J. Tech.* **9**, 105.

WYGNANSKI, I. & FIEDLER, H. 1970 *J. Fluid Mech.* **41**, 327.

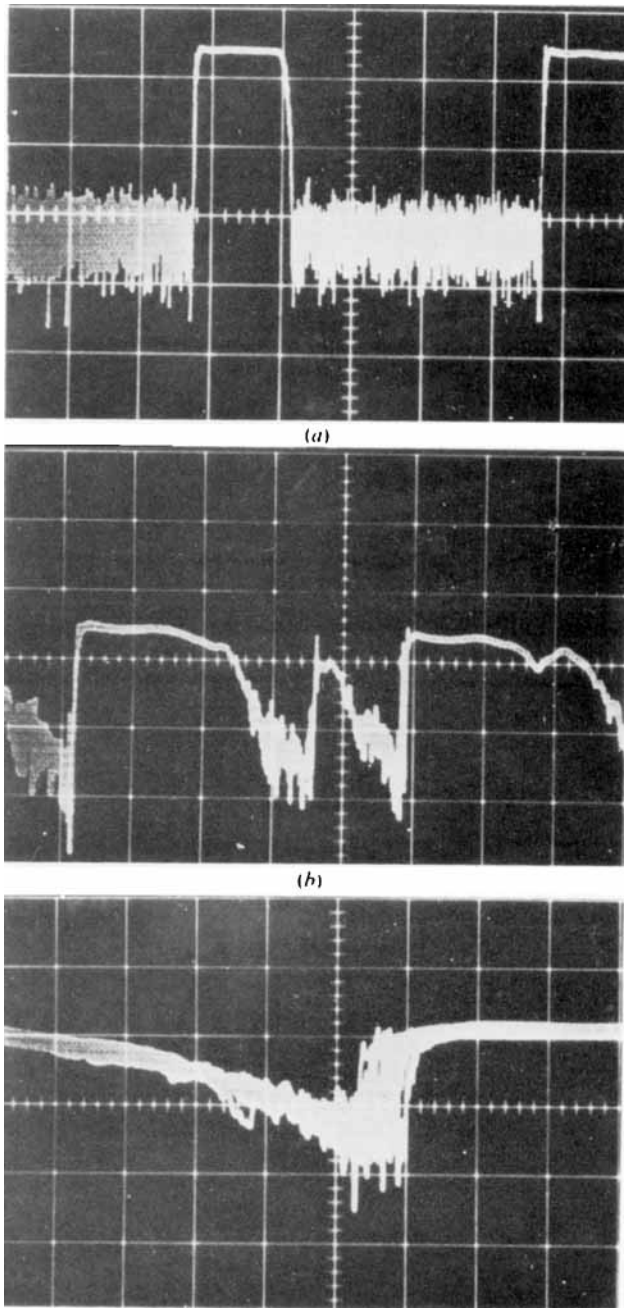

FIGURE 4. Hot-wire traces left by puffs and slugs (vertical scale is proportional to velocity while time runs from left to right). (*a*) Slug; $Re = 4200$, $T = 2$ s/cm. (*b*) Puff; $Re = 2400$, $T = 1$ s/cm. (*c*) Cumulative trace of 15 puffs; $T = 0{\cdot}2$ s/cm.

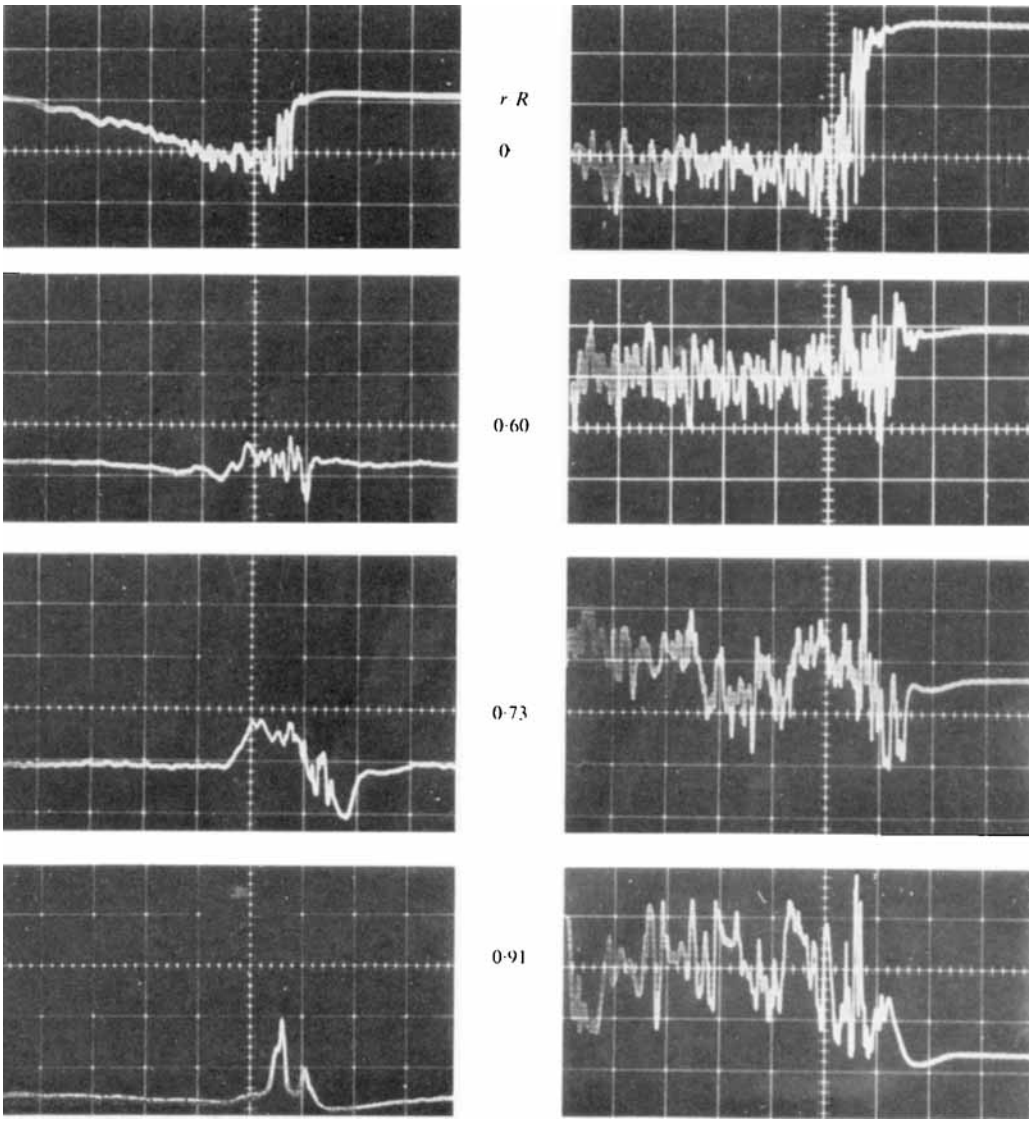

FIGURE 5. Hot-wire traces left by puffs and slugs at various radial locations in the pipe. (*a*) Turbulent puff; $Re = 2360$, $T = 0{\cdot}2$ s/cm. (*b*) Trailing interface of a slug; $Re = 4200$, $T = 0{\cdot}1$ s/cm.

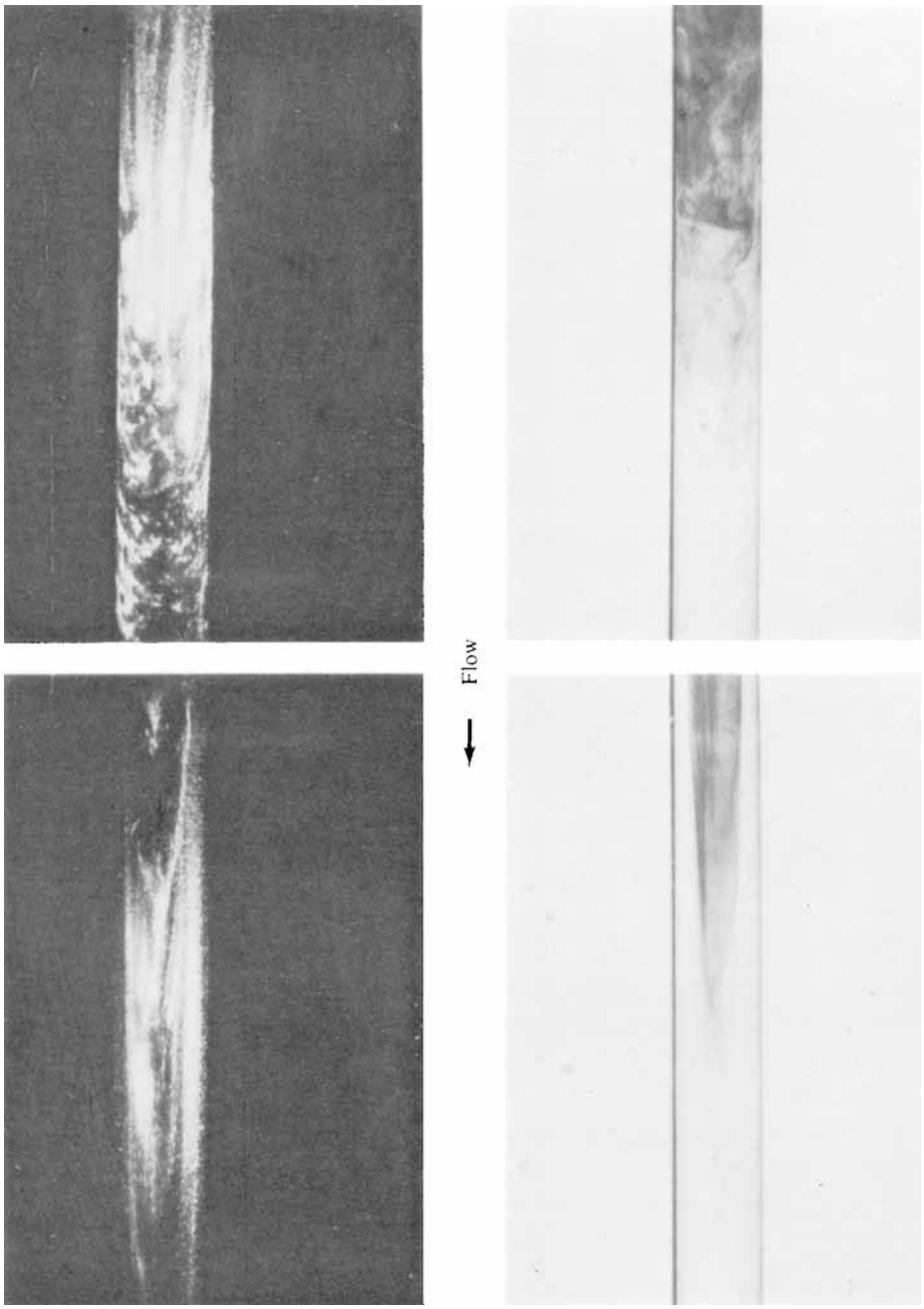

FIGURE 12. Flow visualization downstream of an orifice plate: $Re = 2500$.

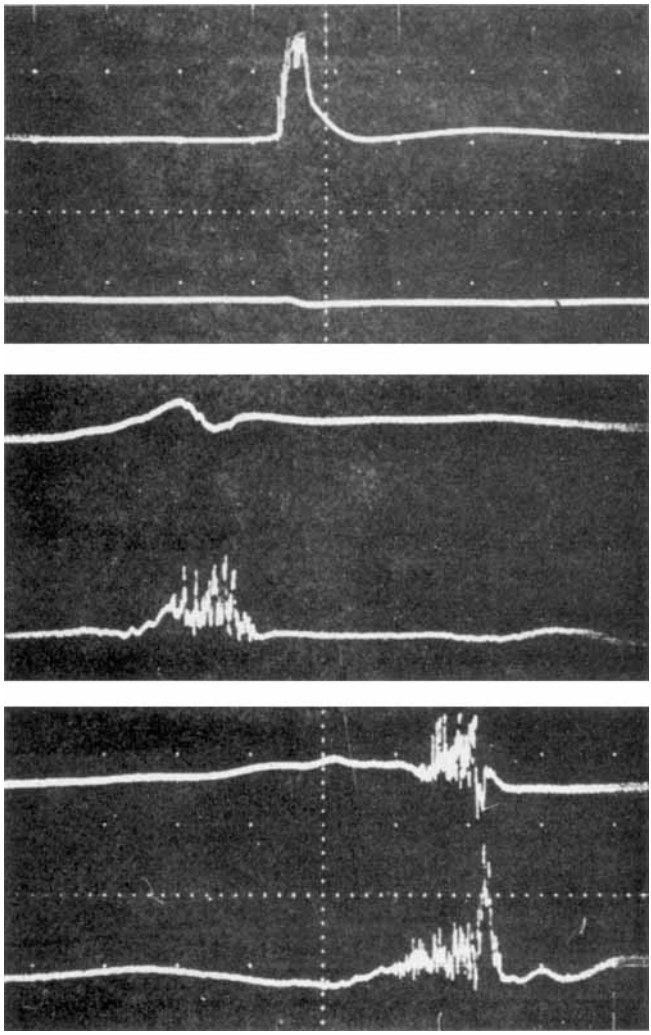

FIGURE 14. Simultaneous traces of two hot-wire outputs placed at opposite and equidistant positions from the centre-line.

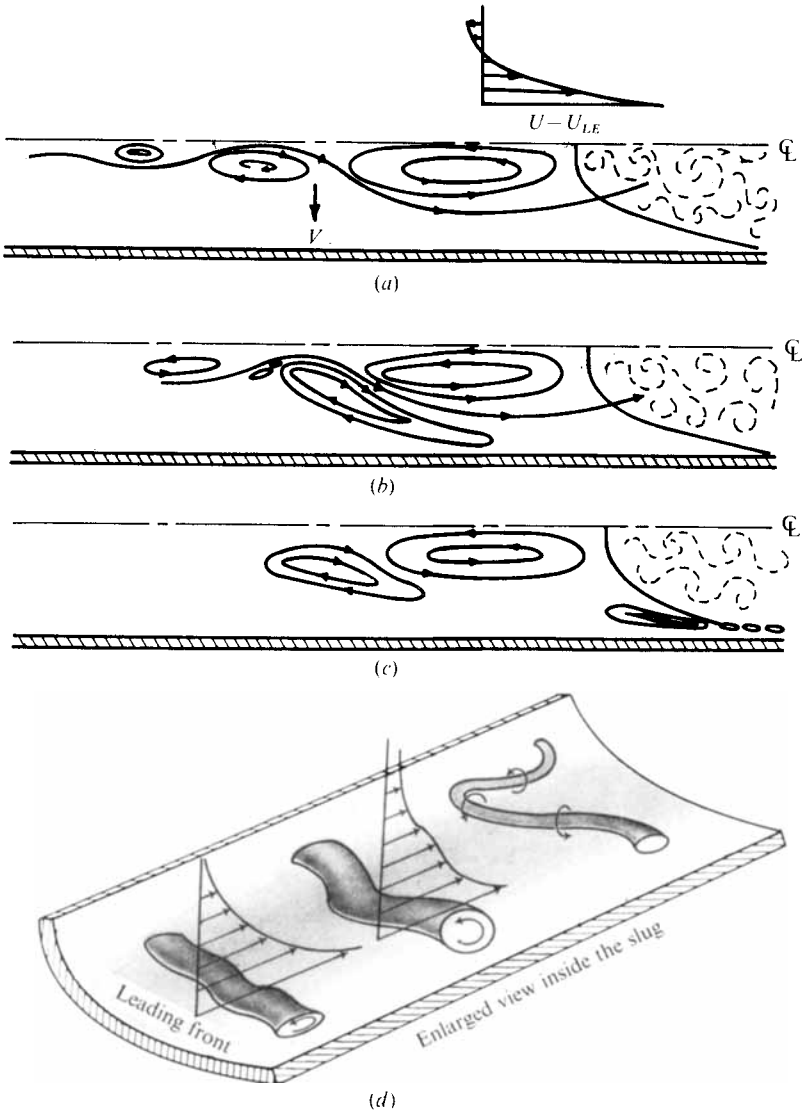

FIGURE 39. A schematic representation of the large eddy structure near the leading interface.

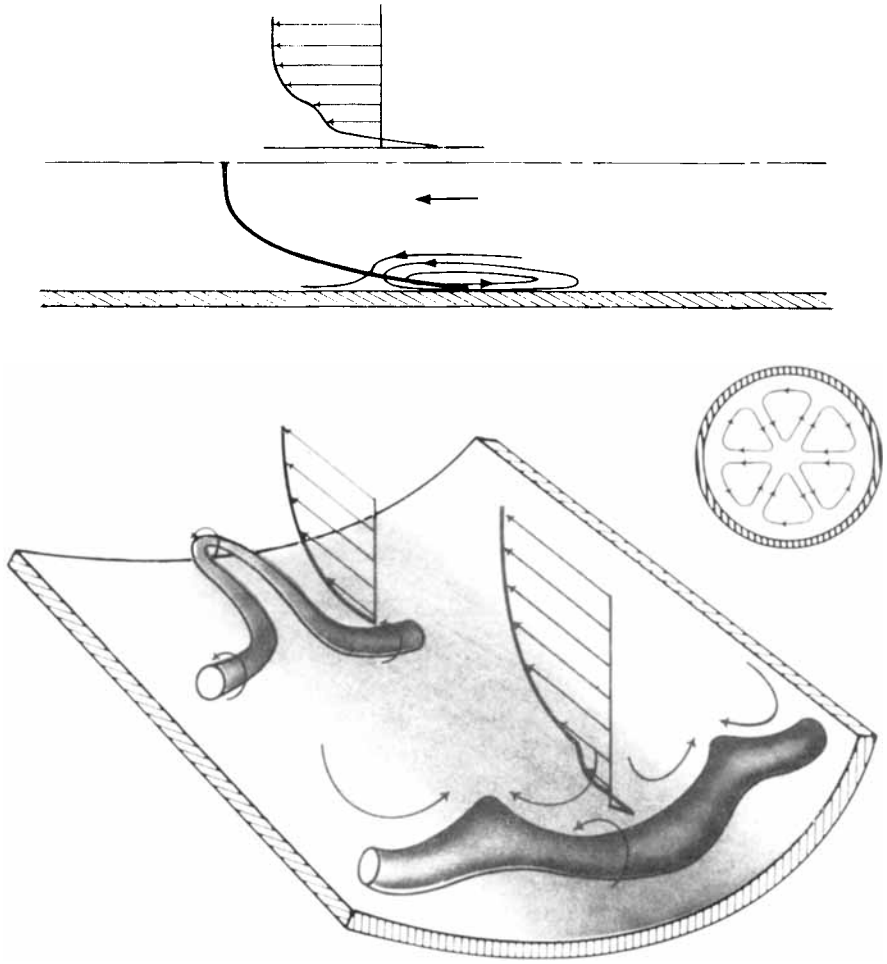

FIGURE 46. A schematic representation of the large eddy structure near the trailing interface.